METABOLIC AND TRANSCRIPTOMIC ANALYSES IDENTIFY COORDINATED RESOURCE REALLOCATION IN RESPONSE TO PHOSPHATE SUPPLY IN HEMP

Benjamin Wee Y.[1,2], Oliver Berkowitz[1,2], Sophia Ng[1,2], Amelia Pegg[1,2], James Whelan[1,3], Ricarda Jost[1,2*]

[1]ARC Research Hub for Medicinal Agriculture, Department of Animal, Plant and Soil Sciences, School of Agriculture, Biomedicine and Environment, La Trobe University, Bundoora VIC 3086, Australia

[2]La Trobe Institute for Sustainable Agriculture & Food, La Trobe University, Bundoora VIC 3086, Australia

[3]College of Life Science, Zhejiang University, Hangzhou, Zhejiang, 310058, P.R. China

Author for correspondence:

Ricarda Jost: r.jost@latrobe.edu.au

Email addresses of authors:

Benjamin Wee Y.: 20826392@students.latrobe.edu.au

Oliver Berkowitz: o.berkowitz@latrobe.edu.au

Sophia Ng: jinqtyan@me.com

Amelia Pegg: a.pegg@latrobe.edu.au

James Whelan: jimwhelan@zju.edu.cn

Ricarda Jost: r.jost@latrobe.edu.au

Number of figures: 6

Number of tables: 0

Word count: 7424

Supplementary data: 2 figures and 7 tables

HIGHLIGHT (30 WORDS)

Contrasting human selection in *Cannabis sativa* enables the analysis of divergent nutrient-use strategies. Our integrated transcriptomic and physiological data revealed adaptive resource allocation, informing the development of nutrient-efficient cultivars.

ABSTRACT

Cannabis sativa L., one of the earliest domesticated crops, was selectively bred into drug-type (high phytocannabinoid yield) and hemp-type (fibre and seed production) varieties, resulting in divergent traits including nutrient requirements. To address the limited molecular understanding of nutrient use regulation in Cannabis, this study investigated the response of dual-purpose hemp to varying phosphate availability. Physiological and transcriptomic profiling across source and sink organs revealed that biomass partitioning to flowers was sustained unless phosphate was completely withdrawn. Analyses of key phosphate-responsive genes highlighted the importance of P reallocation to flowers via glycolytic bypass reactions and release of phosphate from organic pools in source organs. Phospholipid biosynthesis and other P-dependent metabolic pathways remained active in sink organs. While the transcriptional response of key regulators, such as SPX DOMAIN GENE (SPX), PHOSPHATE STARVATION RESPONSE1 (PHR1) and NITRATE-INDUCIBLE, GARP-TYPE TRANSCRIPTIONAL REPRESSOR1 (NIGT1) followed canonical patterns, our data suggest a lack of suppression of phosphate uptake and root-to-shoot translocation at higher phosphate supply levels. Subsequent depletion of nitrate pools restricts further growth. These findings uncover conserved and unique aspects of nutrient signalling in hemp, shedding light on its adaptation to nutrient-poor soils through distinct source–sink regulation.

KEYWORDS

Cannabis sativa, hemp, female flower, nitrogen, phosphorus, sink, source, nutrient use, transcriptomics.

INTRODUCTION

Phosphorus (P) is a critical nutrient for plant growth, influencing a range of physiological processes from gene regulation to energy transfer and flowering (Cho *et al.*, 2025; Ojeda-Rivera *et al.*, 2022). It is exclusively taken up by plant roots in the form of inorganic phosphate (Pi, $H_2PO_4^-$). Despite its importance for metabolism and plant development, research on the molecular regulation of Pi acquisition and use in Cannabis is limited. Understanding the impact of Pi on Cannabis reproductive growth or specialised metabolism is essential to improve biomass and product yield (Lambers, 2021; Xie *et al.*, 2023). P deficiency results in reduced growth, accelerated senescence, and lower cannabinoid content, while excess Pi supply does not enhance biomass production or specialised metabolite accumulation (Cockson *et al.*, 2020; Hershkowitz *et al.*, 2025; Shiponi and Bernstein, 2021b). Notably, cannabinoid concentration in tissues is negatively correlated with Pi supply, while total cannabinoid yield per plant increases with Pi supply due to higher flower biomass (Shiponi and Bernstein, 2021a; Shiponi and Bernstein, 2021b; Wee Y. *et al.*, 2024).

Despite its impact on overall product yield, integration of knowledge gained from physiological responses with available molecular data to characterize the phosphate starvation response (PSR) in Cannabis is limited (Jost *et al.*, 2025; Shiponi and Bernstein, 2021a; Shiponi and Bernstein, 2021b; Wee Y. *et al.*, 2024). The PSR describes a highly complex and conserved regulatory system in plants that controls the coordinated acclimation to low Pi availability through changes in nutrient uptake, root system architecture, and shoot metabolism which has been studied extensively in model plants such as *Arabidopsis*, rice and tomato (Paz-Ares *et al.*, 2022; Péret *et al.*, 2014; Plaxton and Tran, 2011; Yang *et al.*, 2024). MYB transcription factors PHOSPHATE STARVATION RESPONSE1 (PHR1) and PHR1-like orthologs play a key role in PSR, controlling the expression of hundreds of genes containing the P1BS (GnATATnC) cis-regulatory motif in their promoter and enhancer regions (Bustos *et al.*, 2010; Guo *et al.*, 2015; Jiang *et al.*, 2019; Linn *et al.*, 2017; Rubio *et al.*, 2001; Safi *et al.*, 2017). Target genes are associated with processes such as Pi acquisition, e.g., members of the high affinity *PHOSPHATE TRANSPORTER1* (*PHT1*) family, Pi scavenging, e.g., purple acid phosphatases (*PAP*s), and ribonucleases (RNS), assimilation of other nutrients such as iron, sulfate and nitrate as well as membrane lipid remodelling. Release of Pi by phospholipid hydrolysis requires a shift to

62 alternative lipids such as sulfo- and galactolipids. Their synthesis is catalysed by UDP-
63 sulfoquinovose synthases (SQD1 and SQD2), or type B monogalactosyldiacylglycerol
64 (MGD2 and MGD3) and digalactosyldiacylglycerol (DGD2) synthases, respectively
65 (Kelly and Dormann, 2002; Kobayashi *et al.*, 2009; Okazaki *et al.*, 2013; Tjellstrom *et*
66 *al.*, 2008; Yu *et al.*, 2002). PHR1 itself is regulated by SYG1/Pho81/XPR1 (SPX)
67 domain proteins, which bind higher-order inositol pyrophosphates (IPs) to signal
68 cellular phosphorus status (Collins *et al.*, 2024). Other notable transcription factors
69 include WRKY6 and WRKY42, which negatively regulate expression of transcripts
70 encoding Pi exporter and mediator of Pi root-to-shoot translocation, PHOSPHATE1
71 (PHO1), via binding to the W-box motif in the *PHO1* promoter (Chen *et al.*, 2009; Su
72 *et al.*, 2015). At the protein level, PHO1 is negatively regulated by ubiquitin-conjugating
73 E2 enzyme, PHOSPHATE 2 (PHO2) and E3 ligase PRU1 (Liu *et al.*, 2012; Ye *et al.*,
74 2018).
75 Deciphering the interplay between these molecular determinants of PSR and
76 associated physiological responses is essential for advancing development of crop
77 cultivars with high P use efficiency (Gu *et al.*, 2016; Heuer *et al.*, 2017). Given drug-
78 type Cannabis is a high-value medicinal plant largely grown in controlled
79 environments, there has been little effort to improve its P use. This is reflected by
80 differences in nutrient response between usage-types, with drug-type Cannabis
81 exhibiting a tolerance for higher nutrient supplies without yield penalties as opposed
82 to hemp-types, which are generally more nutrient efficient due to being traditionally
83 grown on marginal lands (Scalabrin *et al.*, 2024; Struik *et al.*, 2000; Tang *et al.*, 2018;
84 Wee Y. *et al.*, 2024). These differences underscore the divergent selection of
85 Cannabis for either seed, hurd and fibre or pharmaceutical production. Introgression
86 of a functional *CANNABIDIOLIC ACID SYNTHASE* (*CBDAS*) gene from hemp- into
87 drug-type Cannabis for production of cannabidiol (CBD), has resulted in reintroduction
88 of previously segregated gene combinations (Burgarella *et al.*, 2019; Grassa *et al.*,
89 2021), with noticeable consequences for nutrient use between chemotypes (Jost *et*
90 *al.*, 2024). Comparison of two distinct genotypes representing CBD- and
91 tetrahydrocannabinol (THC)-dominant drug-type cultivars revealed shifts in the
92 expression of some key genes linked to nutrient transport and assimilation, indicating
93 potential trade-offs between cannabinoid biosynthesis and nutrient efficiency.
94 Cannabinoids can represent up to 28% of the dry weight of the female flower as a
95 result of selective breeding for highly productive strains of drug-type Cannabis. In

96 addition, flowers account for up to 70 % of total aboveground biomass, suggesting
97 resource allocation in Cannabis is weighted towards sink.
98 To establish a foundation for our molecular understanding of the PSR in
99 Cannabis, we characterised the morphological, physiological and transcriptomic
100 response of source and sink organs in a dual-purpose hemp cultivar to varying Pi
101 supply. We find that PSR-driven acclimation redirects nutrients and resources to
102 support flower development. In contrast to established crop species, hemp does not
103 downregulate Pi uptake at luxurious supply levels and depletes vacuolar nitrate pools
104 to support P assimilation and growth. Lack of suppression of key molecular PSR
105 components is accompanied by upregulation of high affinity nitrate transporters and
106 genes associated with nitrate assimilation. Our data provide a detailed understanding
107 of the PSR and crosstalk with N assimilation in Cannabis to support the development
108 of strategies for optimizing nutrient use in this multifaceted crop.

109 MATERIALS AND METHODS

110 *Plant material and growth conditions*

111 Photoperiod sensitive Chinese industrial hemp cultivar Han NW bred for seed
112 and fibre production was used to generate mother plant stock via single-seed decent
113 (Clarke, 2020; Welling *et al.*, 2021; Zhang *et al.*, 2021).
114 Female Han NW plants were clonally propagated using 15-cm long cuttings
115 taken from lateral shoots of a mother plant. The base of each cutting was dipped in
116 auxin-enriched gel (Purple Clonex Rooting Hormone Gel, Yates) before transfer into
117 propagation cubes (EasyPlug, Netherlands) pre-saturated with reverse osmosis (RO)-
118 purified water. Cuttings were placed in a seedling tray covered by a humidity dome.
119 Rooting occurred at 24 °C in a controlled environment growth room under long-day
120 conditions (18 h day / 6 h night cycle), with a light intensity of 120 µmol m^{-2} s^{-1}.
121 After two weeks, the most uniform rooted cuttings were transplanted into 0.25
122 L pots containing medium-grade Perlite (P400, Chillagoe Pty Ltd, Australia) and grown
123 under long-day conditions with a light intensity of 200 µmol m^{-2} s^{-1}. Daily fertigation
124 was applied as needed using a modified Hoagland's solution (7.25 mM NO_3^-, 0.25
125 mM NH_4^+, 4.5 mM K, 1 mM Mg, 2 mM Ca, 1 mM S, 20 µM Fe, 2 µM Mn, 2 µM Zn, 25
126 µM Cu, 0.5 µM Co, 0.5 µM Mo, and 25 µM B, with a pH of 6.2) containing 1 mM Pi,
127 with clonal plants receiving a total of 1.8 L in feed and 1.8 mmol Pi.

128 Thirteen days after the first transplant (13 DAT), 15 plants were transferred into
129 4.5 L pots with Perlite P400 substrate and grown for another four weeks under short-
130 day conditions (12 h day / 12 h day-night cycle) with a week-long ramp-up to a final
131 light intensity of 600 µmol m^{-2} s^{-1} to induce flowering. Five Pi treatments were initiated
132 immediately after the transplant, with modified Hoagland's solution containing either
133 0, 0.25, 0.5, 1, or 2 mM KH_2PO_4. Across treatments, potassium levels were maintained
134 at a concentration of 4.5 mM using potassium chloride. Three plants were used in
135 each treatment group (n=3). Fertigation events and volume per event were adjusted
136 to plant development and transpiration, and all plants received the same volume of
137 fertigation mix, which totalled 22.5 L over the entire course of the experiment. All plants
138 were harvest at 42 DAT when female flowers were still immature with white pistillate
139 flower clusters (Punja and Holmes, 2020).

140 ***Sampling***

141 Six different plant organ types (Top Flower (terminal inflorescence), TF; Young
142 Stem, YS; Mature Stem, MS; Young Leaf, YL; Mature Leaf, ML; Old Leaf, OL; Lateral
143 Root, LR) were sampled from each plant at 42 DAT. To ensure consistent phenological
144 definition of leaf types, leaves were pre-selected the day before sampling to ensure
145 similar size, level of lobe expansion, and nodal position along the main stem. YS were
146 sampled from nodes below the TF basal node to the next four lower nodes, while MS
147 were sampled from the node where ML was collected including the next two lower
148 nodes. LR samples were excised from the exterior of the root ball, washed twice with
149 RO water, and dried on paper towels. All samples were shock-frozen in liquid nitrogen,
150 then stored in 15 mL polycarbonate tubes (OPS Diagnostics, USA) at -80 °C, prior to
151 adding a metal grinding ball (∅ 0.5 cm) and processing the frozen material using a
152 Geno/Grinder automated tissue homogenizer (SPEX SamplePrep, USA) for 2 x 1 min
153 at 1450 rpm. Frozen, ground material was stored at -80 °C before being sub-sampled
154 under liquid nitrogen for downstream assays.

155 ***Morphological measurements***

156 Over the course of the experiment, and starting at 1 DAT, measurements of
157 plant height, node count, plant width (widest points of fully extended branches) were
158 taken at indicated time points, while ramification points were recorded from 13 DAT
159 onwards. Ramification points are a measure of shoot branching, as described by

160 Pérez-Harguindeguy *et al.* (2016). For this experiment the 3rd branch from the base of
161 each plant was chosen as representative node.

162 ***Biomass quantification and nutrient efficiency calculations***

163 Plants harvested at 42 DAT were at early flowering stage (terminal racemose
164 inflorescences with white hair-like pistils) (Punja and Holmes, 2020). Plants were
165 separated into flower clusters, leaf and stem for fresh biomass quantification. Root
166 fresh weight was determined following removal of Perlite by two rinses in RO water,
167 followed by a 12-h period of air-drying at room temperature (24 °C). For determination
168 of dry matter, separated organ types were collected in paper bags and dried at 65 °C
169 for approximately seven days to constant weight.

170 From fresh weight, agronomic phosphate-use efficiency (APE) was calculated
171 as plant biomass produced per unit Pi supplied, expressed as g FW $mmol^{-1}$ Pi, using
172 a modified formula adapted from (Neto *et al.*, 2016):

173

174 $$APE = \frac{(FW_{x\ Pi} - FW_{no\ Pi})}{Difference\ in\ the\ total\ available\ Pi\ between\ x\ Pi\ and\ no\ Pi}$$

175

176 $FW_{x\ Pi}$ refers to the average organ fresh weight at a given Pi supply which is
177 compared to that of the respective organ type of a plant that received no Pi. The
178 difference in total Pi supplied to each plant over the experimental period was 5.6, 11.2,
179 22.5 and 44.9 mmol for 0.25, 0.50, 1.0, and 2.0 mM Pi treatments, respectively. Total
180 available Pi (mmol) for the respective Pi treatment was calculated by multiplying the
181 treatment concentration (mM) with the total applied volume (22.5 L), also accounting
182 for 1.8 mmol Pi provided during the 2 weeks of growth in 0.25 L pots prior to transplant
183 at 13 DAT when treatments were initiated.

184 ***Determination of nutrient composition and key metabolites***

185 Aliquots of the frozen ground plant material were used for downstream assays
186 as described in (Jost *et al.*, 2024), unless stated otherwise.

187 One aliquot was used to determine phosphate, sulfate and anthocyanin
188 concentration following a 1% (v/v) acetic extraction at 4 °C in the dark, and
189 centrifugation for 10 min at 20,400 x g and 4 °C. Anthocyanin concentration was
190 determined via the pH differential method (Wrolstad *et al.*, 2005). Free phosphate was
191 quantified using the molybdenum blue method, while sulfate ions were quantified

192 measuring turbidity following precipitation with barium chloride (Ames, 1966;
193 Coutinho, 1996).
194 Nitrate concentration was determined from a second aliquot following water
195 extraction at 80 °C and 500 rpm (ThermoMixer C, Eppendorf). The mixture was then
196 centrifuged for 10 min at 20,400 x g and 22 °C, and supernatants used to quantify
197 nitrate by measuring the yellow complex formed during the nitration of salicylic acid
198 under acidic conditions at 410 nm (Hachiya and Okamoto, 2017).
199 A third aliquot was used to determine chlorophyll, protein and starch following
200 80 % (v/v) ethanol extraction in 10 mM MES buffer pH 5.0 at 70 °C and a 10 min
201 centrifugation at 11,000 x g and 4 °C, carried out in the dark (Hendriks *et al.*, 2003).
202 The supernatant then was used to determine chlorophyll (Lichtenthaler, 1987). The
203 remaining pellet was resuspended in 0.1 mM NaOH at 80 °C and centrifuged as
204 above, with the supernatant used for protein quantification at 595 nm using Coomassie
205 Plus Protein Assay Reagent (Thermo Fisher Scientific, Australia). The remaining pellet
206 was resuspended in 0.5 M HCl in 0.1 M sodium acetate buffer pH 4.9, followed by ON
207 starch hydrolysis at 37 °C. Starch-derived glucose was then quantified in a coupled
208 enzymatic assay using the NADH released by ATP-dependent hexokinase (Hendriks
209 *et al.*, 2003).
210 Elemental composition was analysed via inductively coupled plasma mass
211 spectrometry (ICP-MS) following acid digestion of 10 mg of dried sample in *aqua regia*
212 for 3 hours at 70 °C (Foroughi *et al.*, 2014).
213 Total carbon and nitrogen were quantified using 2 mg of dry plant material,
214 combusted at 1000 °C, with subsequent chemiluminescence detection of nitrous oxide
215 in a 2400 Series II CHNS/O Analyzer (Perkin Elmer, Australia). The reference material
216 for elemental composition and C/N ratio analysis was NIST1573A tomato leaf (Sigma-
217 Aldrich).

218 ***RNA-seq analyses***

219 Total RNA was extracted from ca. 100 mg aliquots of ground frozen material,
220 using the Spectrum Plant Total RNA kit (Sigma-Aldrich) according to the
221 manufacturer's protocol. Removal of gDNA was performed with an On-Column
222 DNaseI digestion kit (Sigma-Aldrich) prior to RNA elution with RNase-free water. RNA-
223 seq library generation and sequencing was performed at the Australian Genome
224 Research Facility (Melbourne) as paired-end 150 bp reads. FastQC software

225 (https://www.bioinformatics.babraham.ac.uk/projects/fastqc/) identified that samples
226 had 95% of reads with an average quality score above 35 and an average of 38 million
227 reads. Transcript read counts were quantified as transcripts per million (TPM) by
228 pseudo-aligning reads against a k-mer index built from the transcript models for the
229 *Cannabis sativa* cs10 reference genome downloaded from the Ensembl Plants
230 database (https://plants.ensembl.org/Cannabis_sativa_female) using the kallisto
231 program with 100 bootstraps (Bray *et al.*, 2016). Differentially expressed genes
232 (DEGs) were then quantified using the sleuth package (Pimentel *et al.*, 2017) and
233 genes with TPM > 10 for at least one organ type across treatments were kept for
234 further downstream analyses. Genes were considered differentially expressed if they
235 had a false discovery rate FDR < 0.05 and the expression difference was greater than
236 two-fold ($|\log_2 FC| > 1$). The ComplexHeatmap package was used to generate
237 heatmaps (Gu, 2022).

238 ***Statistical analyses***

239 All statistical analyses were performed in R (https://www.r-project.org/) by one-
240 way analysis of variance, followed by Tukey's honestly significant difference (HSD)
241 post-hoc test to compare means. To summarize pairwise comparisons from Tukey's
242 HSD test, multcompView package was used to generate compact letter displays
243 (Graves *et al.*, 2015). For comparison of P fractions with plant metabolites, a Pearson
244 correlation matrix was calculated and visualized with corrplot package (Wei and
245 Simko, 2024).

246 **RESULTS**

247 ***Biomass prioritization under varying Pi supply leads to differences in use***
248 ***efficiencies***

249 To characterise the acclimation response to different Pi supply in Cannabis, we
250 firstly determined the biomass allocation to different organs in hemp plants under
251 different Pi supplies. At harvest, visible Pi deficiency symptoms such as stunted
252 growth, chlorosis, and fully senescent mature fan leaves were evident only following
253 complete Pi withdrawal. Plants grown with the lowest Pi supply of 0.25 mM showed
254 limited growth suppression – with growth of younger organs likely supported by higher
255 resource mobilisation from the oldest fan leaves which displayed early senescence as
256 evident by their yellow purplish colour (Figure 1A). Plants grown with higher inputs of

257 Pi showed no premature leaf senescence – but some of the oldest fan leaves along
258 the main stem of plants grown at 1 mM and 2 mM Pi supply were yellowing suggesting
259 nitrogen limitation (Cockson *et al.*, 2019). Plants at the highest Pi supply of 2 mM had
260 smaller leaves which was supported by an average 12% reduction in organ biomass
261 (Supplementary Tables S1 and S2). Root development was similarly constrained, with
262 the largest root systems found in plants treated with 1 mM Pi (Figure 1B,
263 Supplementary Table S1 and 2). The highest shoot-to-root biomass ratio of 2.3 was
264 observed at 0.5 mM Pi supply, while Pi withdrawal reduced this ratio to 1.0 indicating
265 a higher relative resource investment into roots (Supplementary Table S1 and S2).
266 Time-course analysis revealed significant reductions in height and width due to
267 complete Pi withdrawal which became apparent at between 21 and 29 DAT,
268 highlighting delayed response to Pi deficiency (Figure 2A). This contrasts with the
269 faster response time reported in medicinal cannabis (Shiponi and Bernstein, 2021a;
270 Shiponi and Bernstein, 2021b), but aligns with observations in another hemp cultivar
271 Cockson *et al.* (2020). Branching, quantified as the number of ramification points, was
272 particularly sensitive to Pi supply with more pronounced differences between
273 treatments from 35 DAT onwards. Excess Pi supply (2 mM) reduced branching
274 significantly whilst plants supplied with 1 mM Pi continued with lateral shoot outgrowth.
275 Together with the reductions in overall biomass this suggests potential growth
276 constraints due to overaccumulation of Pi.
277 Pi deprivation-triggered resource reallocation towards the root is a trait
278 associated with the PSR in many plant species to enhance Pi acquisition (Lambers *et*
279 *al.*, 2006; Péret *et al.*, 2014). In hemp, a relative increase in root over shoot biomass
280 was only observed under complete Pi withdrawal (Figure 2B, Supplementary Table
281 S1), indicating a low Pi threshold for suppressing foraging responses and confirming
282 the high inherent PUE of hemp (Wee Y. *et al.*, 2024). Pi supply of 0.25 mM was
283 sufficient to shift biomass allocation towards the shoot (Figure 2B), significantly
284 increasing above ground (leaf, stem, flower) over root biomass. At this Pi input,
285 vegetative (leaf, stem) biomass was almost four-fold higher than in P-starved plants,
286 and only 21% lower than in plants treated with 1 mM Pi (Supplementary Table S1). In
287 comparison to Pi-starved plants, flower biomass increased significantly by between
288 six- to eight-fold with Pi supply above 0.25 mM. There were no significant differences
289 in flower biomass between treatments consistent with high inherent PUE in this hemp

290 cultivar – but also indicating that Pi use plateaued at relatively low Pi supplies (Figure
291 2B, Supplementary Table S1).
292 Analysis of agronomic phosphate efficiency (APE) found that 0.25 mM Pi
293 yielded the greatest flower biomass increase per unit of Pi supplied. Plants receiving
294 0.5 mM P did not invest more in root biomass, and their leaves had no visible
295 symptoms of nutrient stress (Figure 2C), corroborating findings from other Cannabis
296 studies (Cockson *et al.*, 2020; Shiponi and Bernstein, 2021a; Shiponi and Bernstein,
297 2021b). These plants also had the most compact growth habit (Figures 1A and 1B).
298 At the two highest Pi supply levels, APE declined for all organ types, suggesting
299 diminishing returns in Pi utilization, likely due to metabolic constraints – and possibly
300 N limitation. Overall, these results indicate that a Pi supply between 0.25 mM and 0.5
301 mM optimises the balance for flower production over vegetative biomass.

302 ***Organ-specific N-limitation with increasing Pi supply***

303 Next, we assessed how varying Pi supply impacted different fractions of P
304 (organic P, Po; inorganic P, Pi) and allocation of other nutrients (nitrate, total nitrogen,
305 sulfate) between different organs (TF, terminal flower; YL, young leaf; ML, mature leaf;
306 OL, old leaf; LR, lateral root; YS, young stem). Significant differences in Pi and Po
307 fractions were observed across organs and treatments ($p < 0.05$) (Figure 3A,
308 Supplementary Table S3). Following Pi withdrawal, plants maintained a minimum
309 intracellular Pi concentration of around 5 μmol g^{-1} FW in aboveground organs
310 regardless of their source or sink identity, indicating that efficient internal Pi recycling
311 and conservation sustain critical metabolic processes under low Pi availability in hemp.
312 In Pi-limited LR however, Pi concentration was as low as 1.1 ± 0.3 μmol g^{-1} FW (Figure
313 3A), likely due to translocation to the shoot. Compared with Pi withdrawal, Pi
314 concentrations increased significantly in most organs under optimal Pi supply (0.5
315 mM), reaching 18.4 ± 1.8 and 8.5 ± 1.5 μmol g^{-1} FW in shoots and roots, respectively.
316 OL contained the lowest amount of total P, indicating resource remobilization (Figure
317 3A). TF were the strongest sinks, with prioritized Pi allocation to flowers maintaining
318 Po levels at 11.8 ± 0.4 μmol g^{-1} FW even under Pi withdrawal – already reaching half
319 (23.8 ± 3.7 μmol g^{-1} FW) of the maximum concentration under limiting Pi supply (≤
320 0.25 mM), and rising to 54.5 ± 6.2 μmol g^{-1} FW under optimal Pi supply (0.5mM). Po
321 levels in different leaf types under Pi limitation (≤ 0.25 mM Pi) remained below 2.1
322 μmol g^{-1} FW, reflecting restricted assimilation of Pi.

323 Preferential Pi translocation into floral organs was further evident from elevated
324 concentrations in YS which retained 14.0 ± 1.2 µmol Pi g^{-1} FW even under Pi
325 withdrawal (Figure 3B), serving as a proxy of sustained active Pi transport to floral
326 organs. By comparison, Pi levels were at least 50% lower in all other organs. Beyond
327 0.5 mM Pi supply, shoot organ concentrations of Pi and Po plateaued, indicating luxury
328 Pi supply and therefore additional metabolic constraints on further Pi utilization.
329 However, in LR, both P fractions steadily increased with Pi supply, suggesting a lack
330 of downregulation in Pi uptake despite sufficient local and systemic P reserves. Lack
331 of downregulation of root Pi uptake and accumulation under sufficient to luxury Pi
332 supply in drug-types was found to be genotype-specific (Jost *et al.*, 2024; Shiponi and
333 Bernstein, 2021b; Wee Y. *et al.*, 2024), while plants such as Arabidopsis, ryegrass
334 and maize effectively restrict further uptake (Penn *et al.*, 2023; Sharma and Sahi,
335 2005; Shukla *et al.*, 2017).
336 Phosphate and sulfate uptake are often tightly and antagonistically coordinated
337 (Clarkson *et al.*, 1992; de Jager *et al.*, 2023; Rouached, 2011). In crop plants, both are
338 usually found at a leaf concentration range of 10 to 20 µmol g^{-1} FW with sulfate linked
339 to PSR-induced lipid remodelling (Blake-Kalff *et al.*, 2000; Cuyas *et al.*, 2023; Prodhan
340 *et al.*, 2017; Suriyagoda *et al.*, 2023; Torres-Rodriguez *et al.*, 2021). Across the Pi
341 supply range, hemp roots contained an average 26 ± 2 µmol g^{-1} FW sulfate suggesting
342 that sulfate uptake and / or translocation are coordinated to maintain a high basal level
343 of sulfate, irrespective of P status (Figure 3B). Conversely, in aboveground organs,
344 sulfate concentrations were trending opposite to phosphate concentrations. P-limited
345 sink organs, particularly TF, accumulated sulfate with concentrations sharply rising
346 from close to detection limit at 0.5 mM Pi supply to 19 ± 1 µmol g^{-1} FW upon Pi
347 withdrawal. In YL, sulfate concentrations were likewise significantly higher at limiting
348 (≤ 0.25 mM) compared with sufficient Pi supplies (≥ 0.5 mM), but did not exceed 11 ±
349 2 µmol g^{-1} FW (Figure 3B). With increasing Pi supply, sulfate concentrations in most
350 shoot organs decreased to less than 1.0 µmol g^{-1} FW, with the notable exception of
351 YS which retained sulfate concentrations of greater than 10 µmol g^{-1} FW up until 0.5
352 mM Pi supply. Increased translocation can also be deduced from the bell-shaped
353 curve in OL with sulfate concentration peaking at 0.5 mM Pi supply (Figure 3B) – most
354 likely due to the slow remobilisation of S during leaf senescence under non-limiting S
355 conditions (Dubousset *et al.*, 2009; Maillard *et al.*, 2015). Higher rates of translocation

356 may indicate that sulfate is still used for partial substitution of phospholipids by
357 sulfolipids under the 0.5 mM Pi treatment. Sulfate concentrations in ML followed a
358 similar Pi supply-dependent trend as those in sink organs but only reached a maximum
359 of 5.2 ± 0.3 µmol g^{-1} FW, which is about four-fold lower than in P-limited TF. In contrast
360 to hemp, sulfate concentrations in *Arabidopsis* increase in P-limited roots, but
361 decrease in the respective shoots (Rouached, 2011; Rouached *et al.*, 2011).
362 N availability in plants is known to affect regulation of PSR genes through
363 crosstalk between nitrate and Pi signalling with low N status suppressing PSR (Hu and
364 Chu, 2020; Poza-Carrion and Paz-Ares, 2019; Torres-Rodriguez *et al.*, 2021; Zhang
365 *et al.*, 2023). Following Pi withdrawal, nitrate concentrations in all but sink organs were
366 high – ranging from 18 ± 8 µmol g^{-1} FW in LR to 80 ± 36 µmol g^{-1} FW in ML - likely due
367 to a higher root-to-shoot ratio and decreased metabolic activity in shoots (Figure 3B).
368 Lower concentrations of 6.0 ± 1.5 µmol g^{-1} FW in TF and 3.5 ± 0.9 µmol g^{-1} FW in YL
369 indicate continued N assimilation in P-limited sink organs. In the presence of as little
370 as 0.25 mM Pi in the nutrient solution, nitrate concentrations dropped sharply across
371 all aboveground organs, ranging from 0.9 – 4.2 µmol g^{-1} FW (Figure 3B), well below
372 adequate concentrations reported in drug-type Cannabis (Jost *et al.*, 2024). Only
373 transport organs (LR, YS) showed a less severe decline in nitrate levels reflecting
374 preferential translocation towards sink organs.
375 Overall, levels of free anions (nitrate, phosphate, and sulfate) suggest N-limited
376 growth across the entire Pi supply range. To further investigate this, we analysed total
377 elemental composition, as well as distribution profiles of key pigments (anthocyanins,
378 chlorophyll) and metabolites (RNA, protein, starch) across organs and treatments
379 (Supplementary Table S3). There were no treatment-specific differences in total C or
380 N concentrations in sink (TF, YL) organs and stems again highlighting active buffering
381 against resource fluctuations (Supplementary (Supplementary Figure S1). Lower total
382 N concentrations in ML at the lowest Pi supply level (0.25 mM) indicate P-limited
383 metabolic activity of source leaves. Accumulation of total N (5-fold) and total C (3-fold)
384 in OL upon Pi withdrawal likely reflects reduced demand from growing sink organs –
385 and storage of N-rich metabolites (e.g., N-rich amino acids, polyamines, proteins) or
386 starch, respectively (Supplementary Figure S1). In LR, a significant two-fold increase
387 in total N under Pi withdrawal is also observed ($p < 0.05$), likely due to increased
388 biomass partitioning towards roots for foraging as previously shown in Figures 1B and

389 1D. Total C, protein and starch levels in roots remain relatively stable across
390 treatments (Supplementary Table S3).
391 Pearson's correlation analysis was used to explore the relationship between
392 quantified metabolites and P fractions, aiming to identify links between P status and
393 the accumulation of these metabolites across organs (Figure 4). In YS, there was a
394 strong positive correlation between Pi and RNA, protein, or starch, showing
395 dependence of metabolic activity on Pi status. This was also true for the correlation
396 between starch and Pi or Po in sink organs (TF, YL), highlighting strong association
397 between Pi availability and carbon fixation. Starch is also known to accumulate
398 because of metabolic constraints under Pi deficiency (MacNeill *et al.*, 2017), but this
399 expected negative correlation with P status was only found in roots (MacNeill *et al.*,
400 2017). Anthocyanin accumulation, a common stress marker in plants (Vance *et al.*,
401 2003), was negatively correlated with Pi in all shoot organs, although this was only
402 statistically significant in ML (Vance *et al.*, 2003). Notably, sink organs (TF, YL)
403 produced more significant correlations compared to source leaves and roots,
404 suggesting a stronger impact of Pi on their metabolic status. This again highlights
405 preferential Pi allocation to these organs (Figure 3B). In sink organs, a strong negative
406 correlation between Pi and Fe was observed, in line with the reported accumulation of
407 chelated iron complexes in P-limited Arabidopsis shoots (Hirsch *et al.*, 2006). In
408 terminal flowers, Ca had an overall negative correlation to Pi, while K and Mg had
409 positive correlations to Pi and / or Po in YL and TF, respectively. These relationships
410 reflect the complex and often antagonistic interactions between Pi and these cations
411 (Devau *et al.*, 2011; Liu *et al.*, 2011; Rietra *et al.*, 2017; Xie *et al.*, 2021; Xie *et al.*,
412 2019). Positive correlation between P and K status in sink organs, especially in YL,
413 agrees with findings in hemp (Cockson *et al.*, 2020) and drug-type Cannabis (Shiponi
414 and Bernstein, 2021b).

415 ***Transcriptional regulation of Phosphate Starvation Response genes implies***
416 ***coordinated metabolic adjustments across source and sink organs***

417 To gain insight into the underlying transcriptional regulation of observed
418 physiological responses, RNA-seq analysis was performed and identified a total of
419 10,327 differentially expressed genes (DEGs) across all organs and treatments
420 compared with Pi supply of 1 mM. Over half of these genes were unique to OL under
421 Pi withdrawal (Supplementary Figure S2 A,B; Supplementary Table S5). GO term

422 enrichment analysis for these genes showed that they are involved in catabolic
423 processes in agreement with the senescence phenotype of OL (Supplementary Figure
424 S2C, Figure 1). To focus on specific responses to Pi availability, these senescence-
425 associated genes were excluded from further analyses.

426 *Pi uptake and translocation*

427 To characterise the transcriptional response in Cannabis, a curated list of genes
428 with known function in the homeostasis and metabolism of Pi in other species was
429 generated (Supplementary Table S6). Six out of nine *PHT1* family homologs identified
430 in hemp were differentially expressed in response to Pi supply in at least one organ
431 type (Figure 5, Supplementary Tables 5 and 6). Their expression profiles suggested a
432 function in increasing root uptake from the soil solution as well as enabling
433 translocation from root to shoot (Wang *et al.*, 2017). The expression of *PHT1*
434 homologs was dependent on Pi supply, with two homologs (*LOC115715182*,
435 *LOC115721935*) being responsive across all organs. Their induction was strongest
436 (up to 962-fold) in Pi-limited source organs (OL and ML), indicating involvement in Pi
437 mobilisation, with weaker induction observed in transport (LR, YS) and sink organs
438 (TF). Pi responses of the other *PHT1* genes were organ-specific, *i.e.*, limited to the
439 root (*LOC115721895*, *LOC115722577*) or to roots and leaves (*LOC115721968*,
440 *LOC115721288*) (Wang *et al.*, 2017). Except for *LOC115721935* and *LOC115722577*,
441 the other Pi responsive *PHT1* homologs maintained a basal level of expression under
442 surplus Pi supply (≥ 1 mM) in LR, likely contributing to the continuous accumulation of
443 Pi (Figure 3A). Supporting PHT1-mediated Pi translocation is the expression of the
444 only *PHOSPHATE TRANSPORTER FACILITATOR1* (*PHF1*) hemp homolog
445 (*LOC115707553*), which is essential for intracellular trafficking of PHT1 from the
446 endoplasmic reticulum to the plasma membrane (Bayle *et al.*, 2011). Under Pi
447 limitation, *CsPHF1* was upregulated by 3- to 9-fold in LR, OL, ML and YS. In line with
448 the sink status of TF, a low, basal expression level was maintained (Figure 5,
449 Supplementary Table S5). In hemp, seven of ten *PHO1(-like)* family members were
450 differentially expressed (Supplementary Table S5), with *LOC115722063* being the
451 closest homolog of the functionally best characterised PHO1 in Arabidopsis (Arpat *et*
452 *al.*, 2012; Hamburger *et al.*, 2002). Even under surplus Pi supply, this gene showed
453 sustained expression in LR and YS, underscoring the sustained transport of Pi towards
454 sink organs driven by PHO1 (Figure 5).

455 Vacuolar Phosphate Efflux (VPE) and SPX- and MFS-domain containing
456 Vacuolar Phosphate Transporter (VPT) / PHT5 family members are responsible for
457 vacuolar Pi efflux and influx, respectively, and play a vital role in intracellular Pi
458 homeostasis. Their expression is induced upon Pi withdrawal in a PHR1-dependent
459 manner (Sun *et al.*, 2023). In hemp, we identified two *VPE* and three *VPT / PHT5*
460 homologs. One hemp *VPE* homolog (*LOC115706709*) was substantially expressed
461 across organs and responsive to Pi limitation (Figure 5, Supplementary Table S5). Its
462 observed upregulation in Pi-starved hemp roots hints at fine tuning of cytosolic Pi pools
463 to ensure that sufficient amounts of Pi are available for xylem loading, which is also
464 observed in rice (Luan *et al.*, 2019; Sun *et al.*, 2023). In rice, *VPE1* and *VPE2* are
465 upregulated under Pi-deficient conditions (Xu *et al.*, 2019). In contrast to Arabidopsis,
466 two of the three *CsVPT* homologs (*LOC115717942*, *LOC115717117*) were mildly Pi
467 responsive in all organs apart from TF. In Arabidopsis, *VPT*s are responsible for
468 vacuolar Pi sequestration and are highly upregulated under Pi-stress to participate in
469 long distance systemic Pi homeostasis (Luan *et al.*, 2019). The response of the third
470 isoform, *LOC115708335*, was more similar to Arabidopsis *AtVPT1*, and showed a
471 more than 1,300-fold induction in Pi-starved roots (Liu *et al.*, 2015; Rose *et al.*, 2016;
472 Yang *et al.*, 2024).

473 *Sensing and Regulation of P status*

474 PHO2, a ubiquitin-conjugating E2 enzyme, is a key regulator of Pi homeostasis
475 suppressing Pi uptake and translocation under P-replete conditions by targeting Pi
476 transporters such as PHO1 and PHT1 for ubiquitin-mediated degradation (Aung *et al.*,
477 2006; Bari *et al.*, 2006; Liu *et al.*, 2012). The E3 ubiquitin ligase NITROGEN
478 LIMITATION ADAPTATION (NLA) works alongside PHO2 to degrade Pi transporters
479 (Lin et al. 2013; Park et al. 2014), as well as PHR1 in response to changes in inositol
480 polyphosphate levels (Park *et al.*, 2023). Out of two PHO2 homologs in hemp, we
481 identified one (*LOC115698240*) with lower transcript abundance in P-limited LR and
482 YS (Figure 5, Supplementary Table S5). Lower transcript levels are consistent with
483 higher Pi transporter and PHR1 activity in these organs, as well as systemic, post-
484 transcriptional regulation of *PHO2* mRNA by miRNA399 observed in Arabidopsis roots
485 (Chiou *et al.*, 2005; Fujii *et al.*, 2005). However, in P-limited source organs (ML, OL),
486 *PHO2* transcript abundance was 3- to 4-fold higher than under P-replete conditions
487 (Figure 5, Supplementary Table S5). This may indicate an additional role of PHO2 in

488 suppressing Pi import into these organs. Like *PHO2*, transcripts encoding the two
489 hemp *NLA* isoforms showed a 3- to 7-fold suppression in P-limited roots, while they
490 were largely unresponsive to Pi-supply in shoots, with one isoform (*LOC115695922*)
491 showing higher constitutive expression across organs.

492 In Arabidopsis and rice, transcript abundance of *PHR1*, the master regulator of
493 the PSR, is largely unresponsive to Pi supply and subject to post-translational
494 regulation by SPX proteins and / or ubiquitin-dependent turnover (Bustos *et al.*, 2010;
495 Nilsson *et al.*, 2007; Park *et al.*, 2023). The closest homolog to *AtPHR1*,
496 *LOC115714052*, was also not transcriptionally responsive to changes in Pi supply
497 (Supplementary Table S7). Two close *PHR1-LIKE* (*PHL*) homologs (*CsPHL13* /
498 *LOC115719175*, *CsPHL1* / *LOC115701526*) were identified in hemp. CsPHL13 had a
499 higher constitutive transcript abundance, especially in roots and leaves, and was
500 responsive to Pi supply with a two-fold induction in P-limited YS (Supplementary Table
501 S5 and S7). By contrast, CsPHL1 expression was very low across organs but showed
502 a 60-fold increased expression in roots supplied with 1 and 2 mM Pi (Figure 5,
503 Supplementary Table S7). Two out of the three *SPX* homologs (*LOC115725567* /
504 *CsSPX1*, *LOC115697978* / *CsSPX3*) were transcriptionally induced across P-limited
505 organs by about 30-fold (Figure 5), similar to corresponding homologs in Arabidopsis,
506 rice and tomato (Puga *et al.*, 2014; Satheesh *et al.*, 2022; Wang *et al.*, 2014). In TF,
507 expression of both *SPX* homologs was five- to seven-fold induced under complete Pi
508 withdrawal only, indicating Pi sufficiency in TF at a Pi supply of 0.25 mM (Figure 5,
509 Supplementary Table S5). Both genes are therefore sensitive indicators of plant P
510 status. Inositol polyphosphates (InsP) influence Pi signalling and homeostasis by
511 regulating SPX-PHR1 interactions (Collins *et al.*, 2024; Ried *et al.*, 2021). In hemp,
512 two putative INOSITOL 1,3,4-TRISPHOSPHATE 5/6-KINASE (ITPK) encoding
513 homologs (*LOC115695287*, *LOC115716459*) were identified, showing organ-specific
514 responses to Pi availability. Notably, transcripts encoding two out of four putative VIP
515 HOMOLOG1 (VIH1) and one VIH2 homolog in hemp showed constitutive expression
516 across organs and were only differentially expressed in P-starved OL (Supplementary
517 Table S5 and S7) (Dong *et al.*, 2019; Laha *et al.*, 2015). In Arabidopsis, ITPK1 and
518 ITPK2 function as key InsP6 kinases to produce inositol pyrophosphates $InsP_7$ and
519 $InsP_8$ in P-sufficient shoots (Riemer *et al.*, 2021). High $InsP_8$ levels stabilize the SPX-
520 PHR1 interaction to keep PHR1 in an inactive state, while Pi stress reduces shoot
521 $InsP_8$ concentration to disrupt SPX-PHR1 binding, thereby allowing PHR1 to bind

522 P1BS motifs and activate PSR genes. In hemp, transcriptional upregulation of the two
523 ITPK homologs in P-limited LR, ML, OL and YS (3- to 11- fold change) is counter-
524 intuitive as this should be associated with reduced PHR1 activity (Figure 5,
525 Supplementary Table S5) (Park *et al.*, 2023).

526 *Mobilisation of Pi from organic compounds by Pi scavenging and lipid remodelling*

527 P-limited plants mobilise Pi by the replacement of membrane phospholipids and
528 breakdown of organic compounds (e.g. phosphate esters), the latter by increasing the
529 activity of phosphatases (PAPs) and ribonucleases (RNSs) and their secretion into the
530 soil (Bariola *et al.*, 1994; Siebers *et al.*, 2015; Tran *et al.*, 2010). Homologs of several
531 genes involved in lipid remodelling were identified and their expression followed a Pi
532 supply dependent pattern across organ types, with some showing the strongest P-
533 limitation responses among all DEGs (Figure 5). Transcripts encoding a
534 phospholipase D (*PLD*, *LOC115718607*) homolog were induced 55- to 3,000-fold in
535 P-limited transport (R, YS) and source (ML, OL) organs, respectively (Supplementary
536 Table 5). The latter corroborates the importance of lipid remodelling in leaves (Li *et*
537 *al.*, 2006). *GLYCEROPHOSPHODIESTER PHOSPHODIESTERASE* (*GDPD)*
538 isoforms are involved in the lipid acyl hydrolase (LAH) pathway of phospholipid
539 hydrolysis and are upregulated under Pi limitation (Mehra *et al.*, 2019). *GDPD*
540 homologs encoded by *LOC115701510* and *LOC115708092* are responsive to Pi
541 supply across all organ types with the former showing more than 3,000-fold induction
542 in P-limited source organs (ML, OL) and YS (Figure 5) and attenuated suppression in
543 P-replete roots compared with other organs. Together with the two *CsSPX* isoforms,
544 *LOC115701510* is thus another sensitive expression marker of P status in Cannabis.
545 *PHOSPHOETHANOLAMINE/PHOSPHOCHOLINE PHOSPHATASE1* (*PECP1*)
546 homologs (*LOC115706703*, *LOC115704970*, *LOC115704930*, *LOC115704928*)
547 encode haloacid dehydrogenase (HAD)-type phosphatases involved in cleaving of Pi
548 from phospholipid polar head groups (Hanchi *et al.*, 2018; Tannert *et al.*, 2018). All
549 three show upregulation under limiting Pi supply across organ types, with strongest
550 induction observed for LOC115704970 and *LOC115704930* in leaves.
551 *LOC115706703* showed a limited transcriptional response to Pi supply but had a
552 higher basal level of expression across organ types, indicating a role in ongoing
553 membrane lipid turnover (Mehra *et al.*, 2019).

554 The protection of sink organs against phospholipid depletion under low Pi
555 supply in hemp is illustrated by the expression patterns of
556 PHOSPHOETHANOLAMINE N-METHYLTRANSFERASE (PEAMT) encoding
557 homologs *LOC115709566* and *LOC115709567*. In *Arabidopsis*, two PEAMT isoforms
558 are involved in *de novo* phospholipid synthesis (Chen *et al.*, 2018). In hemp,
559 transcripts of both *PEAMT* homologs are downregulated by up to 1,200-fold in P-
560 limited sink organs (ML, OL) and YS (Figure 5; Supplementary Table S5). Yet in TF,
561 where Pi is preferentially translocated to (Figure 3A, 3B), expression is largely
562 unaffected, especially for *LOC115709566* which shows a very high transcript
563 abundance in both TF and YS irrespective of external Pi supply. Interestingly, this is
564 opposite to what is observed in Arabidopsis, where *PEAMT* (*NMT1 / PMT1*)
565 expression is upregulated in both roots and shoots to maintain phospholipid synthesis
566 under Pi starvation (Ngo *et al.*, 2022). In aboveground organs of Cannabis,
567 phospholipid synthesis via *PEAMT* is supported only in the presence of sufficient Pi.
568 In P-limited hemp organs where *de novo* phospholipid synthesis via *PEAMT* is limited
569 and phospholipid hydrolysis (*PLD*, *PECP*, *GDPD*) is induced, genes involved in
570 alternative lipid synthesis are also activated. Galactolipid and sulfolipid synthesizing
571 enzymes encoded by *MONOGALACTOSYL DIACYLGLYCEROL SYNTHASE*
572 (*MGD*), DIGALCTOSYLDIACYLGLYCEROL SYNTHASE (*DGD*) and
573 *SULFOQUINOVOSYLDIACYLGLYCEROL SYNTHASE* (*SQD*) genes, respectively,
574 exhibited lower transcriptional activity in sink organs, where phospholipid hydrolysis
575 was similarly constrained (Figure 5). By contrast, roots and leaves showed increased
576 transcriptional activity with a 3- to 720-fold induction of select homologs under limiting
577 Pi supply. Like Arabidopsis, transcripts encoding for one *DGD* homolog
578 (*LOC115706653*) were largely unresponsive to Pi supply, except for P-starved OL –
579 and like AtDGD1, it probably contributes to constitutive galactolipid synthesis in
580 chloroplasts (Kobayashi *et al.*, 2014; Kobayashi *et al.*, 2013), while transcripts of two
581 other homologs (CsMGD2, *LOC115695927*; CsDGD2, *LOC115698658*) are highly Pi
582 responsive in roots and leaves, just like *AtMGD2* and *AtDGD2* (Kelly and Dörmann,
583 2002; Kobayashi *et al.*, 2009). Surprisingly, transcripts encoding the type A MGD
584 synthase CsMGD1 (*LOC115707728*) are induced in P-limited source organs, with a
585 more constitutive expression in YS and TF. This reminiscent of the simultaneous
586 induction of both type A and type B MGD synthase genes observed in sesame plants
587 which are highly tolerant to P impoverished soils (Shimojima *et al.*, 2013). In contrast

588 to the Arabidopsis genes *AtSQD1* and *AtSQD2*, only one *SQD* homolog (*CsSQD2*,
589 *LOC115697608*) was identified in hemp with strong 14- to 30-fold induction in P-limited
590 roots and leaves, respectively. From these expression profiles, *CsSQD2* and *CsMGD2*
591 are another pair of sensitive markers of organ P status (Figure 5, Supplementary Table
592 S5).

593 Pi can also be (re-)mobilised from organic P compounds such as
594 phosphoesters and RNA catalysed by phosphatases (PAP) and ribonucleases (RNS).
595 In Arabidopsis, class I ribonucleases encoding *RNS1* and *RNS2* are upregulated
596 under Pi starvation (Gho *et al.*, 2020; Taylor *et al.*, 1993; Tran *et al.*, 2010). In hemp,
597 two out of six *RNS* homologs were differentially expressed (Figure 5, Supplementary
598 Table S5). Based on their expression profile in hemp, one of the homologs identified,
599 *CsRNS3* (*LOC115698752*), is more similar to Arabidopsis *RNS1*, with strong induction
600 in R, OL and ML, while *CsRNS1* (*LOC115698919*) is more like *AtRNS2* as transcripts
601 are most abundant in P-limited leaves (Bariola *et al.*, 1994; Gho *et al.*, 2020; Taylor *et*
602 *al.*, 1993). Both isoforms exhibit low transcriptional activity in TF, while in YS, a three-
603 to four-fold induction was evident upon Pi withdrawal (Figure 5, Supplementary Table
604 S5). Purple acid phosphatases (PAP*)* are upregulated under Pi stress and play a role
605 in Pi release from intracellular and / or external organic P pools (Bhadouria and Giri,
606 2022). The differentially expressed 15 *PAP* homologs identified in hemp have a similar
607 expression profile to the *RNS* isoforms (Figure 5), with some showing a strong PSR
608 across roots and leaves, while others are more responsive in P-limited leaves. Three
609 *PAP* genes, *CsPAP3* / *LOC115723670*, *CsPAP8* / *LOC115723241*, and *CsPAP17* /
610 *LOC115709102* are good indicators of Pi stress with up to 200-fold induction.

611 ***Altered Pi supply impacts N requirements which is reflected in transcriptional***
612 ***adjustment of nitrate signalling***

613 Pi limitation impacts the homeostasis of other nutrients, especially N, with
614 coordinated regulation at the transcriptional level (Hu and Chu, 2020; Krouk and Kiba,
615 2020; Raven, 2015). In our study, nitrate accumulated significantly in leaves and
616 young stems following Pi withdrawal (Figure 3B). This is unusual given that – in most
617 plants studied - nitrate uptake by roots and its translocation to the shoot are
618 suppressed under Pi limiting conditions (de Magalhães *et al.*, 1998; Gniazdowska and
619 Rychter, 2001; Jeschke *et al.*, 1997; Krouk and Kiba, 2020; Maeda *et al.*, 2018; Ueda
620 and Yanagisawa, 2023; Wang *et al.*, 2020). Total N was significantly increased in P-

621 starved LR and OL only (Supplementary Figure S1), suggesting redirection of N
622 resources to support the observed increase in root-to-shoot ratio (Figure 2B). Under
623 sufficient Pi supply, nitrate concentrations were unexpectedly low, indicative of
624 preferential assimilation into the organic fraction, and likely becoming limiting at higher
625 Pi supplies (Figure 3B, Supplementary Figure S1).

626 We next examined the expression of N regulatory genes as well as of genes
627 encoding steps central to nitrogen uptake and assimilation. An increased demand for
628 N with Pi supply was particularly evident in LR, where expression of *LOC115708988*,
629 one of two *NITRATE TRANSPORTER 3* (*NRT3*) genes encoding a key component of
630 high-affinity nitrate uptake (Okamoto *et al.*, 2006), was steadily induced from 3- to 6-
631 fold as Pi supply was raised from 0.25 mM to 2 mM (Figure 6, Supplementary Table
632 S5 and S6). Transcript profiles of three out of four hemp homologs encoding MADS
633 box transcription factor *ARABIDOPSIS NITRATE REGULATED 1* (*ANR1*) are
634 matching those of *NRT3.1 / LOC115708988* showing root-specific induction with Pi
635 supply (Zhang and Forde, 1998). This induction of nitrate uptake is most likely brought
636 about to match the increased capacity for Pi assimilation and consequently growth
637 (Figure 1). Two-fold induction of a *NITRATE TRANSPORTER 1 (NRT1)/PEPTIDE*
638 *TRANSPORTER* (*NPF*) homolog (*NRT1.2*, *LOC115707825*) in YS with Pi supply
639 points to active transport of nitrate to floral sink organs (Figure 6, Supplementary Table
640 S5 and S7). Increased expression of *NITRATE REDUCTASE* (*NIA*, *LOC115713111*)
641 and *GLUTAMINE SYNTHETASE2* (*GLN2*, LOC115722196) in leaves indicates
642 upregulation of the primary nitrate assimilation pathway to support new growth when
643 P is adequate, which in turn depletes nitrate levels. Transcripts encoding NPF
644 transporter homologs *LOC115699885* (*NPF4.5*, root), *LOC115700848* (*NPF6.4*, leaf),
645 LOC115709842 (NPF2.9, leaf), LOC115710913 (NPF7.3, leaf) were more abundant
646 in P-limited organs. Two nitrite reductase encoding *CsNIR* isoforms (*LOC115702926*,
647 *LOC115702931*), the alpha-subunit of GLUTAMATE DEHYDROGENASE1 encoding
648 *CsGDH1* (*LOC115705444*), and one out of two mitochondrial aspartate
649 aminotransferases encoding loci (*AAT1*, *LOC115699642*) had predominant
650 expression in source organs under Pi withdrawal when nitrate concentrations were
651 high. Reduced suppression of *CsGDH1* in source organs at the highest Pi supply level
652 could be a response to nitrate depletion and increased N metabolic turnover under
653 excess Pi supply. GDH isoforms catalyse both the synthesis and catabolism of
654 glutamate, allowing the (re-)assimilation of ammonia under P or C starvation

655 conditions as well as the generation of N-storage compounds such as N-rich amino
656 acids and polyamines, particularly under high nitrate availability and / or a lack of
657 assimilatory capacity (Forde and Lea, 2007). Contrasts in *CsGLN2* and *CsGDH1*
658 transcript abundance are particularly useful in determining what constitutes a balanced
659 supply of Pi and N for hemp cultivation.

660 Stimulation of nitrate uptake by high P status in hemp is also evident from the
661 transcriptional profile of *NITRATE-INDUCIBLE, GARP-TYPE TRANSCRIPTIONAL*
662 *REPRESSOR1* (*NIGT1*, *LOC115700564*) which suppresses high affinity nitrate
663 acquisition and is also linked to stimulating PSR in Arabidopsis (Medici *et al.*, 2015;
664 Ueda *et al.*, 2020a; Ueda *et al.*, 2020b; Wang *et al.*, 2020). AtNIGT1 shows
665 antagonistic regulation of nitrate transporter gene expression compared with NIN-LIKE
666 PROTEIN (NLP) transcription factors (Maeda *et al.*, 2018). In hemp, *NIGT1* transcript
667 abundance is very low in P-replete organs, particularly in source leaves (ML, OL),
668 while upon Pi withdrawal its expression is upregulated by 8- to 170-fold in ML, OL, and
669 LR, consistent with its role in suppressing nitrate uptake (Figures 3B and 6). In TF and
670 YS, weaker (4.3- to 8-fold) *NIGT1* induction is observed only with Pi withdrawal. As
671 reported in Arabidopsis, *LOC115702149* encoding a NLP6 homolog in hemp shows
672 the opposite expression profile to *NIGT1* (Maeda *et al.*, 2018; Okamoto *et al.*, 2018).
673 Overall, the upregulation of *CsANR1*, *CsNLP6*, and *CsNRT3.1* in P-replete roots,
674 together with *CsNIA*, and *CsGLN2* expression in P-replete shoots is matched by
675 suppression of *CsNIGT1* and *CsGDH1* across those organs. This suggests that in
676 hemp, nitrate uptake and N assimilation are highly responsive to Pi availability. In
677 model organisms such as Arabidopsis, nitrate uptake is likewise counteracted by
678 PHR1-mediated induction of *NIGT1* upon Pi withdrawal, whilst excessive Pi uptake is
679 counteracted by down-regulation of *NIGT1* and promotion of SPX sequestration of
680 PHR1 and NLP (Maeda *et al.*, 2018; Ueda *et al.*, 2020a). In hemp, this seems not to
681 be the case since Pi acquisition is not suppressed by low organ nitrate levels and one
682 putative *PHR1* homolog, *CsPHL13*, even showing transcriptional upregulation with
683 increasing Pi supply in nitrate-depleted source organs (Figure 5).

684 **DISCUSSION**

685 **P utilization efficiency attributed to high Pi recycling and conservation in hemp**

686 Developing optimized fertigation strategies and cultivars balancing nutrient
687 uptake and internal utilization capacity is necessary towards building high-
688 performance Cannabis germplasm (Cockson *et al.*, 2020; Hershkowitz *et al.*, 2025;
689 Heuer *et al.*, 2017; Shiponi and Bernstein, 2021b; Tripathi *et al.*, 2022). In our study,
690 the dual-purpose hemp cultivar showed a remarkable resilience to growth inhibition,
691 requiring complete Pi withdrawal for biomass reallocation away from shoot and
692 reproductive organs towards roots (Figure 2B).

693 The ability of hemp to grow on marginal lands allowed us to study traits for its
694 nutrient-use efficiency (Scalabrin *et al.*, 2024; Wee Y. *et al.*, 2024). This identified key
695 metabolic and transcriptomic acclimation responses in hemp that likely underpin the
696 high PUE. The PSR supports Pi being actively remobilized from roots and source
697 organs towards sink organs, such as flowers (Figure 5). Notably, the young stem
698 serves as a conduit for the efficient translocation of Pi under limiting conditions, with
699 expression closely mirroring that of flowers. These transcriptional changes align very
700 closely with shifts in Pi and Po metabolism across organ types (Figure 3A). Even under
701 limiting Pi supplyng (≤ 0.25 mM Pi), Po concentration in flowers was 70-fold higher
702 than in all other organ types, indicating their protection from nutrient stress as a
703 hallmark of high PUE in hemp. Similar trends have been observed in other sink-heavy
704 crops such as wheat and rice, where reproductive organs accumulate higher P levels
705 to support grain development in genotypes with high PUE (Adem *et al.*, 2020; Aziz *et*
706 *al.*, 2014; Hayes *et al.*, 2022; Irfan *et al.*, 2020; Julia *et al.*, 2016; Suriyagoda *et al.*,
707 2023; Veneklaas *et al.*, 2012).

708 To maintain central processes such as ATP production, nitrogen and carbon
709 assimilation under P limitation, it is essential that alternative pathways are activated in
710 tandem with intracellular Pi-recycling mechanisms (Albinsky *et al.*, 2010; Carstensen
711 *et al.*, 2018; O'Leary *et al.*, 2011). Under Pi stress, we observed a preferential increase
712 in sulfate accumulation in shoot organs. This is in contrast to other plants such as
713 Arabidopsis where sulfate concentrations decrease in shoot organs while increasing
714 in roots (Rouached, 2011). This increased sulfate concentration in shoots under Pi-
715 stress is indicative of how the hemp cultivar complements ongoing Pi reallocation from
716 source to sink organs by transitioning to Pi-free glycerolipids such as sulfo- and

717 galactolipids (Hanchi *et al.*, 2018; Nakamura, 2013; Shimojima *et al.*, 2013; Tjellstrom
718 *et al.*, 2008). As opposed to Arabidopsis where the rate-limiting phospholipid
719 biosynthesis gene *PEAMT* is upregulated under Pi-stress, its expression was
720 positively correlated with Pi supply in hemp (Figure 5) (Chen *et al.*, 2018). Considering
721 that Po levels are maintained even under Pi-limitation in floral organs but not in source
722 organs (Figure 3A), high *PEAMT* transcript abundance irrespective of Pi supply implies
723 *de novo* phospholipid synthesis is supported by preferential Pi translocation to
724 reproductive organs (Aziz *et al.*, 2014). In source organs (ML, OL) where Pi is limiting
725 under Pi stress, PEAMT-mediated phospholipid synthesis is compromised, and
726 expression of genes encoding alternative lipid synthesis dominates. The latter is
727 supported by the decrease in sulfate concentration (Figure 3B) relative to reproductive
728 organs at the same level of Pi supply (Figure 5).
729 Collectively, these two complementary acclimation responses, i.e. enhanced Pi
730 allocation to reproductive sinks and heightened release and turnover of organic P
731 pools through lipid remodelling and phosphatase / nuclease activities, likely underpin
732 the key adaptations that contribute to the high PUE and sustained floral production
733 under Pi-stress in hemp.

734 **Nutrient cross-talk and regulatory implications**

735 This study also revealed that hemp adopts a distinctive strategy for balancing
736 P and N nutrition, differing significantly from canonical models established in, e.g.,
737 *Arabidopsis* and rice. Our results suggest that hemp does not down-regulate Pi uptake
738 and hyperaccumulates Pi in roots and aboveground organs, a trait that is atypical and
739 suggests an alternative mechanism for Pi sensing and translocation that is reminiscent
740 of plants adapted to P impoverished soils like the Australian *Proteacea* and some
741 legumes (Pang *et al.*, 2009; Prodhan *et al.*, 2016; Shane *et al.*, 2004a; Shane *et al.*,
742 2004b). This result is supported by other studies in hemp and drug-type Cannabis
743 (Cockson *et al.*, 2020; Jost *et al.*, 2024; Shiponi and Bernstein, 2021b; Wee Y. *et al.*,
744 2024). The abundance of transcripts encoding the Pi exporter responsible for Pi
745 loading into the xylem, PHO1, supports this observed difference in Pi uptake regulation
746 under excess supply (Figure 5). The dominant *PHO1* gene remains highly expressed
747 in roots and young stems even under high Pi supply, underscoring the strong sink
748 strength of reproductive organs (TF) that drives continuous Pi uptake in roots (Dai *et*
749 *al.*, 2024; Wang *et al.*, 2004). Continued Pi accumulation in roots and stems is in spite

750 of *CsPHO2* upregulation under high Pi supply, which in other plants leads to PHO1
751 degradation to decrease Pi translocation to the shoots - pointing towards a decoupling
752 of the PHO2-PHO1 regulatory axis in hemp (Ouyang *et al.*, 2016). Given that *PHO1*
753 regulates floral transition in both *Arabidopsis* and rice, further investigation into its
754 potential role as a Pi-dependent modulator of flowering time in hemp and drug-type
755 Cannabis is warranted – particularly in cultivars that exhibit elevated *PHO1* expression
756 (Dai *et al.*, 2024).

757 Sustained organ Pi accumulation also raises the important question whether
758 excess Pi uptake in hemp is the result of N limitation as indicated by depleted nitrate
759 storage reserves under Pi-sufficient conditions (Figure 3B). In many plant species,
760 efficient biomass production relies on coordinated nitrate and Pi acquisition, as both
761 are essential for nucleotide and protein biosynthesis (Medici *et al.*, 2019; Pueyo *et al.*,
762 2021; Raven, 2015). Ample supply of nitrate is essential towards activation of PSR
763 genes, whereas nitrate limitation strongly inhibits induction and leads to Pi
764 accumulation along with downregulation of typical PSR genes in crops such as maize,
765 and Arabidopsis (Kant *et al.*, 2011; Maeda *et al.*, 2018; Medici *et al.*, 2015; Schluter *et*
766 *al.*, 2012; Torres-Rodriguez *et al.*, 2021; Wang *et al.*, 2020). In the hemp cultivar, Pi
767 and Po status were negatively correlated with nitrate (Figure 4), despite upregulation
768 of key high affinity nitrate transport system (HATS) component *CsNRT3.1* and
769 corresponding downregulation of its negative GARP-type repressor *CsNIGT1* with
770 increasing Pi supply (Figure 6). Increased N demand with Pi supply is reflected in the
771 upregulation of key nitrate assimilation genes (*NIA, GLN1*) (Figure 6) (Liu *et al.*, 2024;
772 Marschner, 2012; Wang *et al.*, 2002). Yet, remarkably, total N and total C remained
773 unresponsive to Pi supply across aboveground sink organs (Figure 3, Supplementary
774 Figure S1), while the total P and Po fractions – increased with Pi supply (Figure 3).

775 These results suggest that in hemp an increase in Pi supply needs to be
776 carefully balanced with a corresponding higher input of nitrate – as well as
777 photosynthetic activity, to promote synergistic interactions between N and P to support
778 higher stem and / or flower biomass and ultimately target product yield. The observed
779 decoupling of key transcriptional circuits such as PHR1-driven PSR and the PHO2-
780 NLA regulon in hemp, alongside its inverted Pi–N coordination, extends current
781 models of nutrient regulation obtained in other species.

782 Deeper understanding of genotype and usage-type specific nutrient dynamics,
783 helped by the expression profiles of indicative genes identified in our study, has the

784 potential to predict their nutrient use characteristics, enhance cannabinoid production,
785 and support the development of more sustainable cultivation strategies tailored to
786 individual Cannabis germplasm.

787 **SUPPLEMENTARY DATA**

788 **Supplementary Figure 1. Total carbon and nitrogen concentrations in response**
789 **to Pi supply.** Shown are total carbon and nitrogen concentrations across organs and
790 Pi treatments (mean ± SE, n = 3 plants per treatment). Letters denote statistical
791 significance between Pi treatments (ANOVA, Tukey HSD, $p<0.05$).
792

793 **Supplementary Figure 2. Analysis of differentially expressed genes in OL across**
794 **Pi treatments.** Upset plot for differentially expressed genes (DEGs) shared between
795 P-starved organs (**A**) and Venn diagram of DEGs in OL across treatments (**B**) visualise
796 the disproportionate number of DEGs in the OL samples after withdrawal of Pi (P0
797 treatment) due to starvation induced premature senescence. (**C**) Gene ontology (GO)
798 term enrichment analysis for the DEGs specific for the OL of P-starved plants
799 highlights senescence- and proteolysis-related terms in upregulated DEGs, while
800 downregulated DEGs are related to photosynthesis as expected of leaves in the later
801 stages of senescence.
802

803 **Supplementary Table 1: Summary of recorded morphological and physiological**
804 **data.** Sample means and standard errors (SE) were calculated for each variable
805 across the three biological replicates (n) across five treatment groups (0, 0.25, 0.5, 1.0
806 and 2.0 mM Pi). The residual degrees of freedom (df) from one-way ANOVA was used
807 to calculate the upper and lower 95 % confidence limits (CLs) for each variable's
808 pairwise difference in Tukey's HSD test ($p < 0.05$). To summarize pairwise
809 comparisons from Tukey's HSD, compact letter displays (group) were assigned using
810 the *cld* function from package 'multcompView' to generate letter codes, where alpha
811 = 0.5 was used to separate significantly different treatments. df = N-p, where N is the
812 total number of observations (15) and p is the number of parameters estimated (five
813 treatment levels). ADI = Apical dominance index, *i.e.*, number of ramifications per
814 centimetre of representative branch, APE = agronomic phosphate efficiency, DW =
815 dry weight, FW = fresh weight, Internodal Spacing = average distance between nodes
816 along the main stem, SHI = shoot harvest index, S:R = shoot-to-root biomass ratio,
817 Veg = vegetative biomass. Percent scores represent the biomass (FW or DW) of a
818 given organ type as a % of total biomass.
819

820 **Supplementary Table 2**: **Detailed summary of statistical outputs from Tukey's**
821 **HSD following one-way ANOVA for recorded morphological and physiological**
822 **data.** Per variable, treatment pairwise contrasts are given, supplying estimates
823 (difference in group means, *i.e.*, first treatment minus second), pooled standard errors
824 (SE(pooled)) for recorded morphological and physiological data from emmeans Tukey
825 output (pooled, df (residual degrees of freedom), t-statistic (estimate divided by
826 SEpooled)), and adjusted p-values (family-wise error-controlled probabilities from
827 Tukey's HSD for each pairwise contrast). A pooled SE is used because the design is
828 balanced and an assumption of equal variances is assumed. ADI = Apical dominance
829 index, *i.e.*, number of ramifications per centimeter of representative branch, APE =
830 agronomic phosphate efficiency, DW = dry weight, FW = fresh weight, Internodal
831 Spacing = average distance between nodes along the main stem, SHI = shoot harvest
832 index, S:R = shoot-to-root biomass ratio, Veg = vegetative biomass. Percent scores
833 represent the biomass (FW or DW) of a given organ type as a % of total biomass.
834
835 **Supplementary Table 3: Summary of assayed nutrients and metabolites**
836 **alongside statistical analysis by ANOVA followed by Tukey's pairwise**
837 **comparisons, across hemp organs at final destructive harvest.** The residual
838 degrees of freedom (df) from one-way ANOVA was used to calculate the upper and
839 lower 95 % confidence limits (CLs) for each variable's pairwise difference in Tukey's
840 HSD test ($p < 0.05$). To summarize pairwise comparisons from Tukey's HSD, compact
841 letter displays (group) were assigned using the *cld* function from package
842 'multcompView' to generate letter codes, where at alpha=0.05 to separate significantly
843 different treatments. df= N-p, where N is the total number of observations (15) and p
844 is the number of treatment levels (five). C-N ratio = total carbon to nitrogen ratio,
845 organic P= organic phosphorus.
846
847 **Supplementary Table 4**: **Detailed summary of statistical outputs from Tukey's**
848 **HSD following one-way ANOVA for assayed metabolite data, across hemp**
849 **organs at final destructive harvest.** Per variable, pairwise treatment (mM Pi)
850 contrasts are given, supplying estimates (difference in group means, *i.e.*, first
851 treatment minus second), pooled standard errors (SE(pooled)) for recorded
852 morphological and physiological data from emmeans Tukey output, df (residual
853 degrees of freedom), t-statistic (estimate divided by SEpooled)), and adjusted p-values

854 (family-wise error-controlled probabilities from Tukey's HSD for each pairwise
855 contrast). A pooled SE is used because the design is balanced and an assumption of
856 equal variances is assumed. C-N ratio = total carbon to nitrogen ratio, organic P =
857 organic phosphorus.
858
859 **Supplementary Table 5: Summary of DEGs across organs and Pi treatments in**
860 **hemp.** Gene IDs and descriptions are derived from the cs10 genome annotation.
861 Selection criteria applied were as follows: FDR adj. p-value < 0.05, $|\log_2 FC| > 1$, TPM >
862 10 in at least 1 organ type across treatments. Values are provided as $\log_2$ fold-change
863 (logFC) relative to organs of plant treated with 1 mM phosphate (control). Feature =
864 RNA species (m = messenger, nc = non-coding, r = ribosomal, misc = miscellaneous),
865 FDR = false discovery rate with 'NA' indicating lack of statistical significance. "gene
866 family" highlights gene families of special interest, "Pathway annotation" refers to
867 custom annotation.. NA = not available, TF = top flower / terminal inflorescence, ML =
868 mature fan leaf, OL = old fan leaf, YL = young fan leaf, YS = young stem, LR = lateral
869 root. P0 = no phosphate supply, P025 = 0.25 mM phosphate supply, P2 = 2 mM
870 phosphate supply.
871
872 **Supplementary Table 6: Curated list of PSR and other nutrient-response genes**
873 **based on known function in other species.** Gene IDs and descriptions are derived
874 from the cs10 genome annotation. Gene annotations have been verified against
875 Arabidopsis homologs, selecting for the lowest E score (cut-off E<10^-50), and
876 corresponding gene families have also been provided after curation.
877
878 **Supplementary Table 7: Transcripts per million (TPM) values across treatment**
879 **and organ types.** Gene IDs and gene annotations are derived from the cs10 genome
880 annotation. Accession numbers are NCBI RefSeq mRNA transcript identifiers for each
881 predicted transcript model in the cs10 genome annotation. Feature = RNA species (m
882 = messenger, nc = non-coding, r = ribosomal, misc = miscellaneous), TPM =
883 transcripts per million, TF = top flower / terminal inflorescence; ML = mature fan leaf,
884 OL = old fan leaf, YL = young fan leaf, YS = young stem, LR = lateral root. P0 = no
885 phosphate supply, P025 = 0.25 mM phosphate supply, P2 = 2 mM phosphate supply.

886 **ACKNOWLEDGEMENTS**

887 The authors would like to thank Stefanie Kabitz, Filippa Brugliera (both Cann
888 Group Limited) and colleagues within the ARC Industrial Transformation Research
889 Hub for Medicinal Agriculture for useful discussions and feedback.

890 **AUTHOR CONTRIBUTIONS**

891 RJ, OB, JW and BWY conceived the project. BWY conducted the experiment,
892 performed the various assays outlined in the methods as well as data analyses and
893 visualisation. BWY, OB and RJ analysed the data. AP and SN assisted with
894 experimental design and data acquisition. BWY, RJ and OB wrote the manuscript with
895 revision by all authors.
896

897 **CONFLICT OF INTEREST**

898 The authors declare no conflicting interests.

899 **FUNDING**

900 This work was supported by the ARC Industrial Transformation Research Hub
901 for Medicinal Agriculture (JW, grant ID IH180100006).

902 **DATA AVAILABILITY**

903 RNA-seq read data were deposited at the NCBI SRA database under project
904 ID PRJNA1278883.

REFERENCES

905 **Adem GD, Ueda Y, Hayes PE, Wissuwa M**. 2020. Genetic and physiological traits
906 for internal phosphorus utilization efficiency in rice. PLoS One **15**, e0241842.
907 **Albinsky D, Kusano M, Higuchi M, Hayashi N, Kobayashi M, Fukushima A, Mori**
908 **M, Ichikawa T, Matsui K, Kuroda H, Horii Y, Tsumoto Y, Sakakibara H, Hirochika**
909 **H, Matsui M, Saito K**. 2010. Metabolomic screening applied to rice FOX Arabidopsis
910 lines leads to the identification of a gene-changing nitrogen metabolism. Mol Plant **3**,
911 125-142.
912 **Ames B**. 1966. Methods in enzymology. Bd. VIII Complex Carbohydrates: Assay of
913 Inorganic Phosphate, Total Phosphate and Phosphatases.
914 **Arpat AB, Magliano P, Wege S, Rouached H, Stefanovic A, Poirier Y**. 2012.
915 Functional expression of PHO1 to the Golgi and trans-Golgi network and its role in
916 export of inorganic phosphate. The Plant Journal **71**, 479-491.
917 **Aung K, Lin SI, Wu CC, Huang YT, Su CL, Chiou TJ**. 2006. pho2, a phosphate
918 overaccumulator, is caused by a nonsense mutation in a microRNA399 target gene.
919 Plant Physiol **141**, 1000-1011.
920 **Aziz T, Finnegan PM, Lambers H, Jost R**. 2014. Organ-specific phosphorus-
921 allocation patterns and transcript profiles linked to phosphorus efficiency in two
922 contrasting wheat genotypes. Plant, Cell & Environment **37**, 943-960.
923 **Bari R, Datt Pant B, Stitt M, Scheible WR**. 2006. PHO2, microRNA399, and PHR1
924 define a phosphate-signaling pathway in plants. Plant Physiol **141**, 988-999.
925 **Bariola PA, Howard CJ, Taylor CB, Verburg MT, Jaglan VD, Green PJ**. 1994. The
926 Arabidopsis ribonuclease gene RNS1 is tightly controlled in response to phosphate
927 limitation. Plant J **6**, 673-685.
928 **Bayle V, Arrighi J-F, Creff A, Nespoulous C, Vialaret J, Rossignol M, Gonzalez**
929 **E, Paz-Ares J, Nussaume L**. 2011. Arabidopsis thaliana High-Affinity Phosphate
930 Transporters Exhibit Multiple Levels of Posttranslational Regulation The Plant Cell **23**,
931 1523-1535.
932 **Bhadouria J, Giri J**. 2022. Purple acid phosphatases: roles in phosphate utilization
933 and new emerging functions. Plant Cell Rep **41**, 33-51.
934 **Blake-Kalff MMA, Hawkesford MJ, Zhao FJ, McGrath SP**. 2000. Diagnosing sulfur
935 deficiency in field-grown oilseed rape (Brassica napus L.) and wheat (Triticum
936 aestivum L.). Plant and Soil **225**, 95-107.
937 **Bray NL, Pimentel H, Melsted P, Pachter L**. 2016. Near-optimal probabilistic RNA-
938 seq quantification. Nat Biotechnol **34**, 525-527.
939 **Burgarella C, Barnaud A, Kane NA, Jankowski F, Scarcelli N, Billot C, Vigouroux**
940 **Y, Berthouly-Salazar C**. 2019. Adaptive Introgression: An Untapped Evolutionary
941 Mechanism for Crop Adaptation. Front Plant Sci **10**, 4.
942 **Bustos R, Castrillo G, Linhares F, Puga MI, Rubio V, Perez-Perez J, Solano R,**
943 **Leyva A, Paz-Ares J**. 2010. A central regulatory system largely controls
944 transcriptional activation and repression responses to phosphate starvation in
945 Arabidopsis. PLoS Genet **6**, e1001102.
946 **Carstensen A, Herdean A, Schmidt SB, Sharma A, Spetea C, Pribil M, Husted S**.
947 2018. The Impacts of Phosphorus Deficiency on the Photosynthetic Electron Transport
948 Chain. Plant Physiol **177**, 271-284.
949 **Chen W, Salari H, Taylor MC, Jost R, Berkowitz O, Barrow R, Qiu D, Branco R,**
950 **Masle J**. 2018. NMT1 and NMT3 N-Methyltransferase Activity Is Critical to Lipid
951 Homeostasis, Morphogenesis, and Reproduction. Plant Physiol **177**, 1605-1628.

952 **Chen YF, Li LQ, Xu Q, Kong YH, Wang H, Wu WH**. 2009. The WRKY6 transcription
953 factor modulates PHOSPHATE1 expression in response to low Pi stress in
954 Arabidopsis. Plant Cell **21**, 3554-3566.
955 **Chiou T-J, Aung K, Lin S-I, Wu C-C, Chiang S-F, Su C-I**. 2005. Regulation of
956 Phosphate Homeostasis by MicroRNA in Arabidopsis. The Plant Cell **18**, 412-421.
957 **Cho H, Choi I, Bouain N, Nawaz A, Zheng L, Shahzad Z, Brandizzi F, Rhee SY,**
958 **Rouached H**. 2025. Phosphorus Availability Modulates Flowering Time Through
959 Subcellular Reprogramming of bGLU25 and GRP7 in Flowering Plants. bioRxiv,
960 2025.2001.2002.631137.
961 **Clarke RC**. 2020. Tasmania Hemp (Cannabis) Fiber and Seed Cultivar Field Trials—
962 2018-2019. International Journal of Food Science and Agriculture **4**, 470-481.
963 **Clarkson DT, Hawkesford MJ, Davidian J-C, Grignon C**. 1992. Contrasting
964 responses of sulphate and phosphate transport in barley (Hordeum vulgare L.) roots
965 to protein-modifying reagents and inhibition of protein synthesis. Planta **187**, 306-314.
966 **Cockson P, Landis H, Smith T, Hicks K, Whipker BE**. 2019. Characterization of
967 Nutrient Disorders of Cannabis sativa. Applied Sciences **9**, 4432.
968 **Cockson P, Schroeder-Moreno M, Veazie P, Barajas G, Logan D, Davis M,**
969 **Whipker BE**. 2020. Impact of Phosphorus on Cannabis sativa Reproduction,
970 Cannabinoids, and Terpenes. Applied Sciences **10**, 1-18.
971 **Collins E, Shou H, Mao C, Whelan J, Jost R**. 2024. Dynamic interactions between
972 SPX proteins, the ubiquitination machinery, and signalling molecules for stress
973 adaptation at a whole-plant level. Biochem J **481**, 363-385.
974 **Coutinho J**. 1996. Automated method for sulphate determination in soil-plant extracts
975 and waters. Communications in Soil Science and Plant Analysis **27**, 727-740.
976 **Cuyas L, David P, de Craieye D, Ng S, Arkoun M, Plassard C, Faharidine M,**
977 **Hourcade D, Degan F, Pluchon S, Nussaume L**. 2023. Identification and interest of
978 molecular markers to monitor plant Pi status. BMC Plant Biol **23**, 401.
979 **Dai S, Chen H, Shi Y, Xiao X, Xu L, Qin C, Zhu Y, Yi K, Lei M, Zeng H**. 2024.
980 PHOSPHATE1-mediated phosphate translocation from roots to shoots regulates floral
981 transition in plants. J Exp Bot **75**, 5054-5075.
982 **de Jager N, Shukla V, Koprivova A, Lyčka M, Bilalli L, You Y, Zeier J, Kopriva S,**
983 **Ristova D**. 2023. Traits linked to natural variation of sulfur content in Arabidopsis
984 thaliana. Journal of Experimental Botany **75**, 1036-1050.
985 **de Magalhães JV, Alves VMC, de Novais RF, Mosquim PR, Magalhães JR, Filho**
986 **AFCB, Hubert DM**. 1998. Nitrate uptake by corn under increasing periods of
987 phosphorus starvation. Journal of Plant Nutrition **21**, 1753-1763.
988 **Devau N, Hinsinger P, Le Cadre E, Gérard F**. 2011. Root-induced processes
989 controlling phosphate availability in soils with contrasted P-fertilized treatments. Plant
990 and Soil **348**, 203-218.
991 **Dong J, Ma G, Sui L, Wei M, Satheesh V, Zhang R, Ge S, Li J, Zhang TE, Wittwer**
992 **C, Jessen HJ, Zhang H, An GY, Chao DY, Liu D, Lei M**. 2019. Inositol
993 Pyrophosphate InsP(8) Acts as an Intracellular Phosphate Signal in Arabidopsis. Mol
994 Plant **12**, 1463-1473.
995 **Dubousset L, Abdallah M, Desfeux AS, Etienne P, Meuriot F, Hawkesford MJ,**
996 **Gombert J, Segura R, Bataille MP, Reze S, Bonnefoy J, Ameline AF, Ourry A, Le**
997 **Dily F, Avice JC**. 2009. Remobilization of leaf S compounds and senescence in
998 response to restricted sulphate supply during the vegetative stage of oilseed rape are
999 affected by mineral N availability. J Exp Bot **60**, 3239-3253.
1000 **Forde BG, Lea PJ**. 2007. Glutamate in plants: metabolism, regulation, and signalling.
1001 J Exp Bot **58**, 2339-2358.

Foroughi S, Baker AJM, Roessner U, Johnson AAT, Bacic A, Callahan DL. 2014. Hyperaccumulation of zinc by Noccaea caerulescens results in a cascade of stress responses and changes in the elemental profile. Metallomics **6**, 1671-1682.

Fujii H, Chiou T-J, Lin S-I, Aung K, Zhu J-K. 2005. A miRNA Involved in Phosphate-Starvation Response in Arabidopsis. Current Biology **15**, 2038-2043.

Gho YS, Choi H, Moon S, Song MY, Park HE, Kim DH, Ha SH, Jung KH. 2020. Phosphate-Starvation-Inducible S-Like RNase Genes in Rice Are Involved in Phosphate Source Recycling by RNA Decay. Front Plant Sci **11**, 585561.

Gniazdowska A, Rychter AM. 2001. Nitrate uptake by bean (Phaseolus vulgaris L.) roots under phosphate deficiency. In: Gašparíková O, Čiamporová M, Mistrík I, Baluška F, eds. *Recent Advances of Plant Root Structure and Function: Proceedings of the 5th International Symposium on Structure and Function of Roots. Stará Lensná, Slovakia, 30 August – 4 September, 1998*. Dordrecht: Springer Netherlands, 111-117.

Grassa CJ, Weiblen GD, Wenger JP, Dabney C, Poplawski SG, Timothy Motley S, Michael TP, Schwartz CJ. 2021. A new Cannabis genome assembly associates elevated cannabidiol (CBD) with hemp introgressed into marijuana. New Phytol **230**, 1665-1679.

Graves S, Piepho H-P, Selzer ML. 2015. Package 'multcompView'. Visualizations of paired comparisons **451**, 452.

Gu M, Chen A, Sun S, Xu G. 2016. Complex Regulation of Plant Phosphate Transporters and the Gap between Molecular Mechanisms and Practical Application: What Is Missing? Mol Plant **9**, 396-416.

Gu Z. 2022. Complex heatmap visualization. Imeta **1**, e43.

Guo M, Ruan W, Li C, Huang F, Zeng M, Liu Y, Yu Y, Ding X, Wu Y, Wu Z, Mao C, Yi K, Wu P, Mo X. 2015. Integrative Comparison of the Role of the PHOSPHATE RESPONSE1 Subfamily in Phosphate Signaling and Homeostasis in Rice. Plant Physiol **168**, 1762-1776.

Hachiya T, Okamoto Y. 2017. Simple Spectroscopic Determination of Nitrate, Nitrite, and Ammonium in Arabidopsis thaliana. Bio Protoc **7**, e2280.

Hamburger D, Rezzonico E, MacDonald-Comber Petetot J, Somerville C, Poirier Y. 2002. Identification and characterization of the Arabidopsis PHO1 gene involved in phosphate loading to the xylem. Plant Cell **14**, 889-902.

Hanchi M, Thibaud MC, Legeret B, Kuwata K, Pochon N, Beisson F, Cao A, Cuyas L, David P, Doerner P, Ferjani A, Lai F, Li-Beisson Y, Mutterer J, Philibert M, Raghothama KG, Rivasseau C, Secco D, Whelan J, Nussaume L, Javot H. 2018. The Phosphate Fast-Responsive Genes PECP1 and PPsPase1 Affect Phosphocholine and Phosphoethanolamine Content. Plant Physiol **176**, 2943-2962.

Hayes PE, Adem GD, Pariasca-Tanaka J, Wissuwa M. 2022. Leaf phosphorus fractionation in rice to understand internal phosphorus-use efficiency. Ann Bot **129**, 287-302.

Hendriks JH, Kolbe A, Gibon Y, Stitt M, Geigenberger P. 2003. ADP-glucose pyrophosphorylase is activated by posttranslational redox-modification in response to light and to sugars in leaves of Arabidopsis and other plant species. Plant Physiol **133**, 838-849.

Hershkowitz JA, Westmoreland FM, Bugbee B. 2025. Elevated root-zone P and nutrient concentration do not increase yield or cannabinoids in medical cannabis. Front Plant Sci **16**, 1433985.

Heuer S, Gaxiola R, Schilling R, Herrera-Estrella L, López-Arredondo D, Wissuwa M, Delhaize E, Rouached H. 2017. Improving phosphorus use efficiency: a complex trait with emerging opportunities. The Plant Journal **90**, 868-885.

1052 **Hirsch J, Marin E, Floriani M, Chiarenza S, Richaud P, Nussaume L, Thibaud MC**.
1053 2006. Phosphate deficiency promotes modification of iron distribution in Arabidopsis
1054 plants. Biochimie **88**, 1767-1771.
1055 **Hu B, Chu C**. 2020. Nitrogen-phosphorus interplay: old story with molecular tale. New
1056 Phytol **225**, 1455-1460.
1057 **Irfan M, Aziz T, Maqsood MA, Bilal HM, Siddique KHM, Xu M**. 2020. Phosphorus
1058 (P) use efficiency in rice is linked to tissue-specific biomass and P allocation patterns.
1059 Sci Rep **10**, 4278.
1060 **Jeschke WD, Kirkby EA, Peuke AD, Pate JS, Hartung W**. 1997. Effects of P
1061 deficiency on assimilation and transport of nitrate and phosphate in intact plants of
1062 castor bean (Ricinus communis L.). Journal of Experimental Botany **48**, 75-91.
1063 **Jiang M, Sun L, Isupov MN, Littlechild JA, Wu X, Wang Q, Wang Q, Yang W, Wu**
1064 **Y**. 2019. Structural basis for the Target DNA recognition and binding by the MYB
1065 domain of phosphate starvation response 1. FEBS J **286**, 2809-2821.
1066 **Jost R, Berkowitz O, Pegg A, Hurgobin B, Tamiru-Oli M, Welling MT, Deseo MA,**
1067 **Noorda H, Brugliera F, Lewsey MG, Doblin MS, Bacic AT, Whelan J**. 2024. Sink
1068 strength, nutrient allocation, cannabinoid yield and associated transcript profiles vary
1069 in two drug-type Cannabis chemovars. Journal of Experimental Botany.
1070 **Jost R, Schilling S, Melzer R**. 2025. Improving medicinal plant cultivation through in-
1071 depth understanding of environmental, physiological, metabolic, and genetic
1072 constraints. J Exp Bot **76**, 1-4.
1073 **Julia C, Wissuwa M, Kretzschmar T, Jeong K, Rose T**. 2016. Phosphorus uptake,
1074 partitioning and redistribution during grain filling in rice. Ann Bot **118**, 1151-1162.
1075 **Kant S, Peng M, Rothstein SJ**. 2011. Genetic regulation by NLA and microRNA827
1076 for maintaining nitrate-dependent phosphate homeostasis in arabidopsis. PLoS Genet
1077 **7**, e1002021.
1078 **Kelly AA, Dormann P**. 2002. DGD2, an arabidopsis gene encoding a UDP-galactose-
1079 dependent digalactosyldiacylglycerol synthase is expressed during growth under
1080 phosphate-limiting conditions. J Biol Chem **277**, 1166-1173.
1081 **Kelly AA, Dörmann P**. 2002. DGD2, an Arabidopsis Gene Encoding a UDP-
1082 Galactose-dependent Digalactosyldiacylglycerol Synthase Is Expressed during
1083 Growth under Phosphate-limiting Conditions*. Journal of Biological Chemistry **277**,
1084 1166-1173.
1085 **Kobayashi K, Awai K, Nakamura M, Nagatani A, Masuda T, Ohta H**. 2009. Type-B
1086 monogalactosyldiacylglycerol synthases are involved in phosphate starvation-induced
1087 lipid remodeling, and are crucial for low-phosphate adaptation. Plant J **57**, 322-331.
1088 **Kobayashi K, Fujii S, Sasaki D, Baba S, Ohta H, Masuda T, Wada H**. 2014.
1089 Transcriptional regulation of thylakoid galactolipid biosynthesis coordinated with
1090 chlorophyll biosynthesis during the development of chloroplasts in Arabidopsis.
1091 Frontiers in Plant Science **Volume 5 - 2014**.
1092 **Kobayashi K, Narise T, Sonoike K, Hashimoto H, Sato N, Kondo M, Nishimura**
1093 **M, Sato M, Toyooka K, Sugimoto K, Wada H, Masuda T, Ohta H**. 2013. Role of
1094 galactolipid biosynthesis in coordinated development of photosynthetic complexes
1095 and thylakoid membranes during chloroplast biogenesis in Arabidopsis. Plant J **73**,
1096 250-261.
1097 **Krouk G, Kiba T**. 2020. Nitrogen and Phosphorus interactions in plants: from
1098 agronomic to physiological and molecular insights. Curr Opin Plant Biol **57**, 104-109.
1099 **Laha D, Johnen P, Azevedo C, Dynowski M, Weiß M, Capolicchio S, Mao H, Iven**
1100 **T, Steenbergen M, Freyer M, Gaugler P, de Campos MKF, Zheng N, Feussner I,**
1101 **Jessen HJ, Van Wees SCM, Saiardi A, Schaaf G**. 2015. VIH2 Regulates the

Synthesis of Inositol Pyrophosphate InsP8 and Jasmonate-Dependent Defenses in Arabidopsis. The Plant Cell **27**, 1082-1097.

Lambers H. 2021. Phosphorus Acquisition and Utilization in Plants. Annu Rev Plant Biol.

Lambers H, Shane MW, Cramer MD, Pearse SJ, Veneklaas EJ. 2006. Root structure and functioning for efficient acquisition of phosphorus: Matching morphological and physiological traits. Ann Bot **98**, 693-713.

Li M, Qin C, Welti R, Wang X. 2006. Double knockouts of phospholipases Dzeta1 and Dzeta2 in Arabidopsis affect root elongation during phosphate-limited growth but do not affect root hair patterning. Plant Physiol **140**, 761-770.

Lichtenthaler HK. 1987. [34] Chlorophylls and carotenoids: Pigments of photosynthetic biomembranes. *Methods in Enzymology*, Vol. 148: Academic Press, 350-382.

Linn J, Ren M, Berkowitz O, Ding W, van der Merwe MJ, Whelan J, Jost R. 2017. Root Cell-Specific Regulators of Phosphate-Dependent Growth. Plant Physiol **174**, 1969-1989.

Liu J, Yang L, Luan M, Wang Y, Zhang C, Zhang B, Shi J, Zhao FG, Lan W, Luan S. 2015. A vacuolar phosphate transporter essential for phosphate homeostasis in Arabidopsis. Proc Natl Acad Sci U S A **112**, E6571-6578.

Liu T-Y, Aung K, Tseng C-Y, Chang T-Y, Chen Y-S, Chiou T-J. 2011. Vacuolar Ca2+/H+ Transport Activity Is Required for Systemic Phosphate Homeostasis Involving Shoot-to-Root Signaling in Arabidopsis Plant Physiology **156**, 1176-1189.

Liu TY, Huang TK, Tseng CY, Lai YS, Lin SI, Lin WY, Chen JW, Chiou TJ. 2012. PHO2-dependent degradation of PHO1 modulates phosphate homeostasis in Arabidopsis. Plant Cell **24**, 2168-2183.

Liu Z, Huang S, Zhu L, Li C, Zhang D, Chen M, Liu Y, Zhang Y. 2024. PHR1 negatively regulates nitrate reductase activity by directly inhibiting the transcription of NIA1 in Arabidopsis. Journal of Plant Physiology **303**, 154382.

Luan M, Zhao F, Han X, Sun G, Yang Y, Liu J, Shi J, Fu A, Lan W, Luan S. 2019. Vacuolar Phosphate Transporters Contribute to Systemic Phosphate Homeostasis Vital for Reproductive Development in Arabidopsis. Plant Physiol **179**, 640-655.

MacNeill GJ, Mehrpouyan S, Minow MAA, Patterson JA, Tetlow IJ, Emes MJ. 2017. Starch as a source, starch as a sink: the bifunctional role of starch in carbon allocation. J Exp Bot **68**, 4433-4453.

Maeda Y, Konishi M, Kiba T, Sakuraba Y, Sawaki N, Kurai T, Ueda Y, Sakakibara H, Yanagisawa S. 2018. A NIGT1-centred transcriptional cascade regulates nitrate signalling and incorporates phosphorus starvation signals in Arabidopsis. Nat Commun **9**, 1376.

Maillard A, Diquelou S, Billard V, Laine P, Garnica M, Prudent M, Garcia-Mina JM, Yvin JC, Ourry A. 2015. Leaf mineral nutrient remobilization during leaf senescence and modulation by nutrient deficiency. Front Plant Sci **6**, 317.

Marschner H. 2012. *Marschner's Mineral Nutrition of Higher Plants*.

Medici A, Marshall-Colon A, Ronzier E, Szponarski W, Wang R, Gojon A, Crawford NM, Ruffel S, Coruzzi GM, Krouk G. 2015. AtNIGT1/HRS1 integrates nitrate and phosphate signals at the Arabidopsis root tip. Nat Commun **6**, 6274.

Medici A, Szponarski W, Dangeville P, Safi A, Dissanayake IM, Saenchai C, Emanuel A, Rubio V, Lacombe B, Ruffel S, Tanurdzic M, Rouached H, Krouk G. 2019. Identification of Molecular Integrators Shows that Nitrogen Actively Controls the Phosphate Starvation Response in Plants. Plant Cell **31**, 1171-1184.

Mehra P, Pandey BK, Verma L, Giri J. 2019. A novel glycerophosphodiester phosphodiesterase improves phosphate deficiency tolerance in rice. Plant Cell Environ **42**, 1167-1179.

Nakamura Y. 2013. Phosphate starvation and membrane lipid remodeling in seed plants. Prog Lipid Res **52**, 43-50.

Neto AP, Favarin JL, Hammond JP, Tezotto T, Couto HT. 2016. Analysis of Phosphorus Use Efficiency Traits in Coffea Genotypes Reveals Coffea arabica and Coffea canephora Have Contrasting Phosphorus Uptake and Utilization Efficiencies. Front Plant Sci **7**, 408.

Ngo AH, Angkawijaya AE, Lin YC, Liu YC, Nakamura Y. 2022. The phospho-base N-methyltransferases PMT1 and PMT2 produce phosphocholine for leaf growth in phosphorus-starved Arabidopsis. J Exp Bot **73**, 2985-2994.

Nilsson L, Muller R, Nielsen TH. 2007. Increased expression of the MYB-related transcription factor, PHR1, leads to enhanced phosphate uptake in Arabidopsis thaliana. Plant Cell Environ **30**, 1499-1512.

O'Leary B, Park J, Plaxton WC. 2011. The remarkable diversity of plant PEPC (phosphoenolpyruvate carboxylase): recent insights into the physiological functions and post-translational controls of non-photosynthetic PEPCs. Biochem J **436**, 15-34.

Ojeda-Rivera JO, Alejo-Jacuinde G, Najera-Gonzalez HR, Lopez-Arredondo D. 2022. Prospects of genetics and breeding for low-phosphate tolerance: an integrated approach from soil to cell. Theor Appl Genet.

Okamoto M, Kumar A, Li W, Wang Y, Siddiqi MY, Crawford NM, Glass ADM. 2006. High-Affinity Nitrate Transport in Roots of Arabidopsis Depends on Expression of the NAR2-Like Gene AtNRT3.1. Plant Physiology **140**, 1036-1046.

Okamoto Y, Suzuki T, Sugiura D, Kiba T, Sakakibara H, Hachiya T. 2018. Shoot nitrate underlies a perception of nitrogen satiety to trigger local and systemic signaling cascades in
Arabidopsis thaliana. Soil Science and Plant Nutrition **65**, 56-64.

Okazaki Y, Otsuki H, Narisawa T, Kobayashi M, Sawai S, Kamide Y, Kusano M, Aoki T, Hirai MY, Saito K. 2013. A new class of plant lipid is essential for protection against phosphorus depletion. Nat Commun **4**, 1510.

Ouyang X, , Hong X, , Zhao X, , Zhang W, , He X, , Ma W, , Teng W, , Tong Y, . 2016. Knock out of the PHOSPHATE 2 Gene TaPHO2-A1 Improves Phosphorus Uptake and Grain Yield under Low Phosphorus Conditions in Common Wheat. Scientific Reports **6**, 1-11.

Pang J, Tibbett M, Denton MD, Lambers H, Siddique KHM, Bolland MDA, Revell CK, Ryan MH. 2009. Variation in seedling growth of 11 perennial legumes in response to phosphorus supply. Plant and Soil **328**, 133-143.

Park SH, Jeong JS, Huang CH, Park BS, Chua NH. 2023. Inositol polyphosphates-regulated polyubiquitination of PHR1 by NLA E3 ligase during phosphate starvation response in Arabidopsis. New Phytol **237**, 1215-1228.

Paz-Ares J, Puga MI, Rojas-Triana M, Martinez-Hevia I, Diaz S, Poza-Carrión C, Miñambres M, Leyva A. 2022. Plant adaptation to low phosphorus availability: Core signaling, crosstalks, and applied implications. Mol Plant **15**, 104-124.

Penn CJ, Camberato JJ, Wiethorn MA. 2023. How Much Phosphorus Uptake Is Required for Achieving Maximum Maize Grain Yield? Part 1: Luxury Consumption and Implications for Yield. Agronomy **13**, 95.

Péret B, Desnos T, Jost R, Kanno S, Berkowitz O, Nussaume L. 2014. Root Architecture Responses: In Search of Phosphate. Plant Physiol **166**, 1713-1723.

Pérez-Harguindeguy N, Díaz S, Garnier E, Lavorel S, Poorter H, Jaureguiberry P, Bret-Harte MS, Cornwell WK, Craine JM, Gurvich DE, Urcelay C, Veneklaas EJ, Reich PB, Poorter L, Wright IJ, Ray P, Enrico L, Pausas JG, de Vos AC, Buchmann N, Funes G, Quétier F, Hodgson JG, Thompson K, Morgan HD, ter Steege H, Sack L, Blonder B, Poschlod P, Vaieretti MV, Conti G, Staver AC, Aquino S, Cornelissen JHC. 2016. Corrigendum to: New handbook for standardised measurement of plant functional traits worldwide. Australian Journal of Botany **64**.

Pimentel H, Bray NL, Puente S, Melsted P, Pachter L. 2017. Differential analysis of RNA-seq incorporating quantification uncertainty. Nat Methods **14**, 687-690.

Plaxton WC, Tran HT. 2011. Metabolic adaptations of phosphate-starved plants. Plant Physiol **156**, 1006-1015.

Poza-Carrion C, Paz-Ares J. 2019. When nitrate and phosphate sensors meet. Nat Plants **5**, 339-340.

Prodhan MA, Jost R, Watanabe M, Hoefgen R, Lambers H, Finnegan PM. 2016. Tight control of nitrate acquisition in a plant species that evolved in an extremely phosphorus-impoverished environment. Plant Cell Environ **39**, 2754-2761.

Prodhan MA, Jost R, Watanabe M, Hoefgen R, Lambers H, Finnegan PM. 2017. Tight control of sulfur assimilation: an adaptive mechanism for a plant from a severely phosphorus-impoverished habitat. New Phytol **215**, 1068-1079.

Pueyo JJ, Quinones MA, Coba de la Pena T, Fedorova EE, Lucas MM. 2021. Nitrogen and Phosphorus Interplay in Lupin Root Nodules and Cluster Roots. Front Plant Sci **12**, 644218.

Puga MI, Mateos I, Charukesi R, Wang Z, Franco-Zorrilla JM, de Lorenzo L, Irigoyen ML, Masiero S, Bustos R, Rodriguez J, Leyva A, Rubio V, Sommer H, Paz-Ares J. 2014. SPX1 is a phosphate-dependent inhibitor of Phosphate Starvation Response 1 in Arabidopsis. Proc Natl Acad Sci U S A **111**, 14947-14952.

Punja ZK, Holmes JE. 2020. Hermaphroditism in Marijuana (Cannabis sativa L.) Inflorescences – Impact on Floral Morphology, Seed Formation, Progeny Sex Ratios, and Genetic Variation. Front Plant Sci **11**, 718.

Raven JA. 2015. Interactions between Nitrogen and Phosphorus metabolism. *Annual Plant Reviews Volume 48*, 187-214.

Ried MK, Wild R, Zhu J, Pipercevic J, Sturm K, Broger L, Harmel RK, Abriata LA, Hothorn LA, Fiedler D, Hiller S, Hothorn M. 2021. Inositol pyrophosphates promote the interaction of SPX domains with the coiled-coil motif of PHR transcription factors to regulate plant phosphate homeostasis. Nat Commun **12**, 384.

Riemer E, Qiu D, Laha D, Harmel RK, Gaugler P, Gaugler V, Frei M, Hajirezaei MR, Laha NP, Krusenbaum L, Schneider R, Saiardi A, Fiedler D, Jessen HJ, Schaaf G, Giehl RFH. 2021. ITPK1 is an InsP(6)/ADP phosphotransferase that controls phosphate signaling in Arabidopsis. Mol Plant **14**, 1864-1880.

Rietra RPJJ, Heinen M, Dimkpa CO, Bindraban PS. 2017. Effects of Nutrient Antagonism and Synergism on Yield and Fertilizer Use Efficiency. Communications in Soil Science and Plant Analysis **48**, 1895-1920.

Rose T, Kretzschmar T, Liu L, Lancaster G, Wissuwa M. 2016. Phosphorus Deficiency Alters Nutrient Accumulation Patterns and Grain Nutritional Quality in Rice. Agronomy **6**.

Rouached H. 2011. Multilevel coordination of phosphate and sulfate homeostasis in plants. Plant Signal Behav **6**, 952-955.

Rouached H, Secco D, Arpat B, Poirier Y. 2011. The transcription factor PHR1 plays a key role in the regulation of sulfate shoot-to-root flux upon phosphate starvation in Arabidopsis. BMC Plant Biol **11**, 19.

Rubio V, Linhares F, Solano R, Martin AC, Iglesias J, Leyva A, Paz-Ares J. 2001. A conserved MYB transcription factor involved in phosphate starvation signaling both in vascular plants and in unicellular algae. Genes Dev **15**, 2122-2133.

Safi A, Medici A, Szponarski W, Ruffel S, Lacombe B, Krouk G. 2017. The world according to GARP transcription factors. Curr Opin Plant Biol **39**, 159-167.

Satheesh V, Zhang J, Li J, You Q, Zhao P, Wang P, Lei M. 2022. High transcriptome plasticity drives phosphate starvation responses in tomato. Stress Biol **2**, 18.

Scalabrin E, Radaelli M, Capodaglio G, Pierobon M, Del Vecchio S, Buffa G. 2024. Hemp cultivation opportunities for marginal lands development. PLoS One **19**, e0299981.

Schluter U, Mascher M, Colmsee C, Scholz U, Brautigam A, Fahnenstich H, Sonnewald U. 2012. Maize source leaf adaptation to nitrogen deficiency affects not only nitrogen and carbon metabolism but also control of phosphate homeostasis. Plant Physiol **160**, 1384-1406.

Shane MW, McCully ME, Lambers H. 2004a. Tissue and cellular phosphorus storage during development of phosphorus toxicity in Hakea prostrata (Proteaceae). Journal of Experimental Botany **55**, 1033-1044.

Shane MW, Szota C, Lambers H. 2004b. A root trait accounting for the extreme phosphorus sensitivity of Hakea prostrata (Proteaceae). Plant, Cell & Environment **27**, 991-1004.

Sharma NC, Sahi SV. 2005. Characterization of Phosphate Accumulation in Lolium multiflorum for Remediation of Phosphorus-Enriched Soils. Environmental Science & Technology **39**, 5475-5480.

Shimojima M, Watanabe T, Madoka Y, Koizumi R, Yamamoto MP, Masuda K, Yamada K, Masuda S, Ohta H. 2013. Differential regulation of two types of monogalactosyldiacylglycerol synthase in membrane lipid remodeling under phosphate-limited conditions in sesame plants. Front Plant Sci **4**, 469.

Shiponi S, Bernstein N. 2021a. Response of medical cannabis (Cannabis sativa L.) genotypes to P supply under long photoperiod: Functional phenotyping and the ionome. Industrial Crops and Products **161**.

Shiponi S, Bernstein N. 2021b. The Highs and Lows of P Supply in Medical Cannabis: Effects on Cannabinoids, the Ionome, and Morpho-Physiology. Front Plant Sci **12**.

Shukla D, Rinehart CA, Sahi SV. 2017. Comprehensive study of excess phosphate response reveals ethylene mediated signaling that negatively regulates plant growth and development. Scientific Reports **7**, 1-16.

Siebers M, Dörmann P, Hölzl G. 2015. Membrane remodelling in phosphorus-deficient plants. *Annual Plant Reviews Volume 48*, 237-263.

Struik PC, Amaducci S, Bullard MJ, Stutterheim NC, Venturi G, Cromack HTH. 2000. Agronomy of fibre hemp (Cannabis sativa L.) in Europe. Industrial Crops and Products **11**, 107-118.

Su T, Xu Q, Zhang FC, Chen Y, Li LQ, Wu WH, Chen YF. 2015. WRKY42 modulates phosphate homeostasis through regulating phosphate translocation and acquisition in Arabidopsis. Plant Physiol **167**, 1579-1591.

Sun G, Luan M, Wen J, Wang B, Lan W. 2023. Genetically controlling VACUOLAR PHOSPHATE TRANSPORTER 1 contributes to low-phosphorus seeds in Arabidopsis. Plant Signal Behav **18**, 2186641.

Suriyagoda LDB, Ryan MH, Gille CE, Dayrell RLC, Finnegan PM, Ranathunge K, Nicol D, Lambers H. 2023. Phosphorus fractions in leaves. New Phytol **237**, 1122-1135.

1300 **Tang K, Fracasso A, Struik PC, Yin X, Amaducci S**. 2018. Water- and Nitrogen-Use
1301 Efficiencies of Hemp (Cannabis sativa L.) Based on Whole-Canopy Measurements
1302 and Modeling. Front Plant Sci **9**, 951.
1303 **Tannert M, May A, Ditfe D, Berger S, Balcke GU, Tissier A, Kock M**. 2018. Pi
1304 starvation-dependent regulation of ethanolamine metabolism by
1305 phosphoethanolamine phosphatase PECP1 in Arabidopsis roots. J Exp Bot **69**, 467-
1306 481.
1307 **Taylor CB, Bariola PA, delCardayré SB, Raines RT, Green PJ**. 1993. RNS2: a
1308 senescence-associated RNase of Arabidopsis that diverged from the S-RNases
1309 before speciation. Proceedings of the National Academy of Sciences **90**, 5118-5122.
1310 **Tjellstrom H, Andersson MX, Larsson KE, Sandelius AS**. 2008. Membrane
1311 phospholipids as a phosphate reserve: the dynamic nature of phospholipid-to-
1312 digalactosyl diacylglycerol exchange in higher plants. Plant Cell Environ **31**, 1388-
1313 1398.
1314 **Torres-Rodriguez JV, Salazar-Vidal MN, Chavez Montes RA, Massange-Sanchez**
1315 **JA, Gillmor CS, Sawers RJH**. 2021. Low nitrogen availability inhibits the phosphorus
1316 starvation response in maize (Zea mays ssp. mays L.). BMC Plant Biol **21**, 259.
1317 **Tran HT, Hurley BA, Plaxton WC**. 2010. Feeding hungry plants: The role of purple
1318 acid phosphatases in phosphate nutrition. Plant Science **179**, 14-27.
1319 **Tripathi R, Tewari R, Singh KP, Keswani C, Minkina T, Srivastava AK, De Corato**
1320 **U, Sansinenea E**. 2022. Plant mineral nutrition and disease resistance: A significant
1321 linkage for sustainable crop protection. Front Plant Sci **13**, 883970.
1322 **Ueda Y, Kiba T, Yanagisawa S**. 2020a. Nitrate-inducible NIGT1 proteins modulate
1323 phosphate uptake and starvation signalling via transcriptional regulation of SPX
1324 genes. Plant J **102**, 448-466.
1325 **Ueda Y, Nosaki S, Sakuraba Y, Miyakawa T, Kiba T, Tanokura M, Yanagisawa S**.
1326 2020b. NIGT1 family proteins exhibit dual mode DNA recognition to regulate nutrient
1327 response-associated genes in Arabidopsis. PLoS Genet **16**, e1009197.
1328 **Ueda Y, Yanagisawa S**. 2023. Transcription factor module NLP-NIGT1 fine-tunes
1329 NITRATE TRANSPORTER2.1 expression. Plant Physiol **193**, 2865-2879.
1330 **Vance CP, Stone CU, Allan DL**. 2003. Phosphorus acquisition and use: critical
1331 adaptations by plants for securing a nonrenewable resource. New Phytol **157**, 423-
1332 447.
1333 **Veneklaas EJ, Lambers H, Bragg J, Finnegan PM, Lovelock CE, Plaxton WC,**
1334 **Price CA, Scheible WR, Shane MW, White PJ, Raven JA**. 2012. Opportunities for
1335 improving phosphorus-use efficiency in crop plants. New Phytol **195**, 306-320.
1336 **Wang D, Lv S, Jiang P, Li Y**. 2017. Roles, Regulation, and Agricultural Application of
1337 Plant Phosphate Transporters. Front Plant Sci **8**, 817.
1338 **Wang X, Wang HF, Chen Y, Sun MM, Wang Y, Chen YF**. 2020. The Transcription
1339 Factor NIGT1.2 Modulates Both Phosphate Uptake and Nitrate Influx during
1340 Phosphate Starvation in Arabidopsis and Maize. Plant Cell **32**, 3519-3534.
1341 **Wang Y, Ribot C, Rezzonico E, Poirier Y**. 2004. Structure and expression profile of
1342 the Arabidopsis PHO1 gene family indicates a broad role in inorganic phosphate
1343 homeostasis. Plant Physiol **135**, 400-411.
1344 **Wang YH, Garvin DF, Kochian LV**. 2002. Rapid induction of regulatory and
1345 transporter genes in response to phosphorus, potassium, and iron deficiencies in
1346 tomato roots. Evidence for cross talk and root/rhizosphere-mediated signals. Plant
1347 Physiol **130**, 1361-1370.
1348 **Wang Z, Ruan W, Shi J, Zhang L, Xiang D, Yang C, Li C, Wu Z, Liu Y, Yu Y, Shou**
1349 **H, Mo X, Mao C, Wu P**. 2014. Rice SPX1 and SPX2 inhibit phosphate starvation

responses through interacting with PHR2 in a phosphate-dependent manner. Proc Natl Acad Sci U S A **111**, 14953-14958.

Wee Y. B, Berkowitz O, Whelan J, Jost R. 2024. Same, Yet Different: Towards Understanding Nutrient Use In Hemp- And Drug-Type Cannabis. Journal of Experimental Botany.

Wei T, Simko V. 2024. R package 'corrplot': Visualization of a Correlation Matrix.

Welling MT, Deseo MA, Bacic A, Doblin MS. 2021. Untargeted Metabolomic Analyses Reveal Chemical Complexity of Dioecious Cannabis Flowers. Australian Journal of Chemistry **74**, 463-479.

Wrolstad RE, Durst RW, Lee J. 2005. Tracking color and pigment changes in anthocyanin products. Trends in food science & technology **16**, 423-428.

Xie K, Cakmak I, Wang S, Zhang F, Guo S. 2021. Synergistic and antagonistic interactions between potassium and magnesium in higher plants. The Crop Journal **9**, 249-256.

Xie X, Hu W, Fan X, Chen H, Tang M. 2019. Frontiers | Interactions Between Phosphorus, Zinc, and Iron Homeostasis in Nonmycorrhizal and Mycorrhizal Plants. Frontiers in Plant Science **10**.

Xie Z, Mi Y, Kong L, Gao M, Chen S, Chen W, Meng X, Sun W, Chen S, Xu Z. 2023. Cannabis sativa: origin and history, glandular trichome development, and cannabinoid biosynthesis. Hortic Res **10**, uhad150.

Xu L, Zhao H, Wan R, Liu Y, Xu Z, Tian W, Ruan W, Wang F, Deng M, Wang J, Dolan L, Luan S, Xue S, Yi K. 2019. Identification of vacuolar phosphate efflux transporters in land plants. Nat Plants **5**, 84-94.

Yang SY, Lin WY, Hsiao YM, Chiou TJ. 2024. Milestones in understanding transport, sensing, and signaling of the plant nutrient phosphorus. Plant Cell **36**, 1504-1523.

Ye Q, Wang H, Su T, Wu W-H, Chen Y-F. 2018. The Ubiquitin E3 Ligase PRU1 Regulates WRKY6 Degradation to Modulate Phosphate Homeostasis in Response to Low-Pi Stress in Arabidopsis. The Plant Cell **30**, 1062-1076.

Yu B, Xu C, Benning C. 2002. Arabidopsisdisrupted in SQD2encoding sulfolipid synthase is impaired in phosphate-limited growth. Proceedings of the National Academy of Sciences **99**, 5732-5737.

Zager JJ, Lange I, Srividya N, Smith A, Lange BM. 2019. Gene Networks Underlying Cannabinoid and Terpenoid Accumulation in Cannabis. Plant Physiol **180**, 1877-1897.

Zhang H, Forde BG. 1998. An Arabidopsis MADS Box Gene That Controls Nutrient-Induced Changes in Root Architecture. Science **279**, 407-409.

Zhang M, Anderson SL, Brym ZT, Pearson BJ. 2021. Photoperiodic Flowering Response of Essential Oil, Grain, and Fiber Hemp (Cannabis sativa L.) Cultivars. Front Plant Sci **12**, 694153.

Zhang Z, Zhong Z, Xiong Y. 2023. Sailing in complex nutrient signaling networks: Where I am, where to go, and how to go? Mol Plant.

FIGURE LEGENDS:

Figure 1. Phenotypic response of female hemp plants to changes in Pi supply. Shown are images of representative clonal plants for each treatment prior to final destructive harvest at 42 DAT. (**A**) Plant morphology across treatments. Chlorosis gradient increased in senescing leaves along the main stem with decreasing Pi supply. Scale bar represents 20 cm. (**B**) Root ball morphology across treatments. Scale bar represents 5 cm. Organ biomass in g FW plant^{-1} is given below each panel, as mean ± SE (n = 3 plants per treatment).

Figure 2. Morphological response to Pi supply across timepoints. (**A**) Changes in plant height, plant width and node count were determined at indicated time points across treatments. DAT refers to days after transfer of rooted female cuttings into pots. Arrows indicate timepoint when Pi treatments were initiated. (**B**) Biomass partitioning across organ types, as a percentage of total fresh biomass for each treatment. Vegetative organs are stem and leaves combined. (**C**) Agronomic phosphate efficiency (APE) across treatments in comparison to 0 mM Pi supply. APE is highest at 0.25 mM Pi supply and decreases with higher Pi supply across organs. Given are means ± SE, n = 3 plants per treatment. Letters denote significant difference (ANOVA, Tukey's HSD, $p < 0.05$) between treatments and / or organ types. Also refer to Supplementary Table S1 and S2 for supporting datasets.

Figure 3. Pi supply affects Pi assimilation as well as inorganic storage pools across organ types. (**A**) Concentrations of inorganic and organic P across organ types and Pi treatments. (**B**) Concentrations of nitrate, phosphate and sulfate across organ types and Pi treatments. Letters denote statistical significance across treatments (ANOVA/TUKEY HSD, $p < 0.05$). Given are means ± SE (n = 3 plants per treatment). See Supplementary Table S3 for data and statistical analyses. TF, terminal flower; YL, young leaf; ML, mature leaf; OL, old leaf; LR, lateral root; YS, young stem.

Figure 4. Correlation matrix of measured metabolites and P fractions across organ types. Pearson's correlation to assess relationship between concentrations of indicated metabolites and different P fractions for given organs. Asterisks denote

significant correlations ($p < 0.05$) and colour scale indicates correlation coefficient. ND: not determined.

Figure 5. Transcriptional response of curated PSR genes. Cannabis homologs of known PSR genes in Arabidopsis were categorised into functional groups. PSR transcript abundances across organ types (LR, lateral root; OL, old leaf, ML, mature leaf; YS, young stem; TF, terminal flower) and Pi treatments (0, 0.25, 1, 2 mM Pi) are expressed as $\log_2$ transformed TPM values. Transcriptomic data and curated gene list are provided in Supplementary Table S5 to S7. The cs10 reference referenc gene IDs are shown on the right. Abbreviations for gene family names shown to the left of the panel: *PHT, PHOSPHATE TRANSPORTER; PHF1, PHOSHATE TRANSPORT FACILITATOR1; PHO1, PHOSPHATE1; VPE, VACUOLAR PHOSPHATE EFFLUX TRANSPORTER; VPT, VACUOLAR PHOSPHATE TRANSPORTER; PHO2, PHOSPHATE2; NLA, NITROGEN LIMITATION ADAPTATION; PHR1, PHOSPHATE STARVATION RESPONSE1; SPX, SPX DOMAIN GENE; ITPK, INOSITOL 1,3,4-TRISPHOSPHATE 5/6-KINASE; WRKY, WRKY DNA-BINDING PROTEIN; MYB, MYB-DOMAIN PROTEIN; RNS, RIBONUCLEASE; PAP, PURPLE ACID PHOSPHATASE; PLD, PHOSPHOLIPASE D; GDPD, GLYCEROPHOSPHODIESTER PHOSPHODIESTERASE; PECP1, PHOSPHOETHANOLAMINE/PHOSPHOCHOLINE PHOSPHATASE1; PEAMT, PHOSPHOETHANOLAMINE N-METHYLTRANSFERASE; MGD, MONO-GALACTOSYL DIACYLGLYCEROL SYNTHASE; SQD, SULFOQUINOVOSYL-DIACYLGLYCEROL SYNTHASE*.

Figure 6. Transcriptionalresponse of curated genes involved in N assimilation and metabolism in hemp. Shown are transcript abundances for Cannabis homologs of genes with a known role in N assimilation, metabolism and their transcriptional regulation in Arabidopsis. The heatmap represents log-transformed TPM ($\log_2$(TPM+1)) across organ types (LR, lateral root; OL, old leaf, ML, mature leaf; YS, young stem; TF, terminal flower). Transcriptomic dataset and fully curated gene list is provided in Supplementary Table S5-S7. cs10 genome gene IDs are shown on the right. Abbreviations for gene family names shown on the left of the panel: *AMT, AMMONIUM TRANSPORTER; NRT, NITRATE TRANSPORTER; ANR1, ARABIDOPSIS NITRATE REGULATED1; NITRITE REDUCTASE, NIR; NITRATE*

REDUCTASE, NIA; GLUTAMINE SYNTHETASE, GLN; NITRATE-INDUCIBLE GARP-TYPE TRANSCRIPTIONAL REPRESSOR1, NIGT1; NIN-LIKE PROTEIN, NLP; NRT1/PEPTIDE TRANSPORTER, NPF; GLUTAMATE DEHYDROGENASE, GDH; ASPARTATE AMINOTRANSFERASE, AAT; C-TERMINALLY ENCODED PEPTIDE, CEP; CALCINEURIN B-LIKE PROTEIN-INTERACTING PROTEIN KINASE, CIPK.

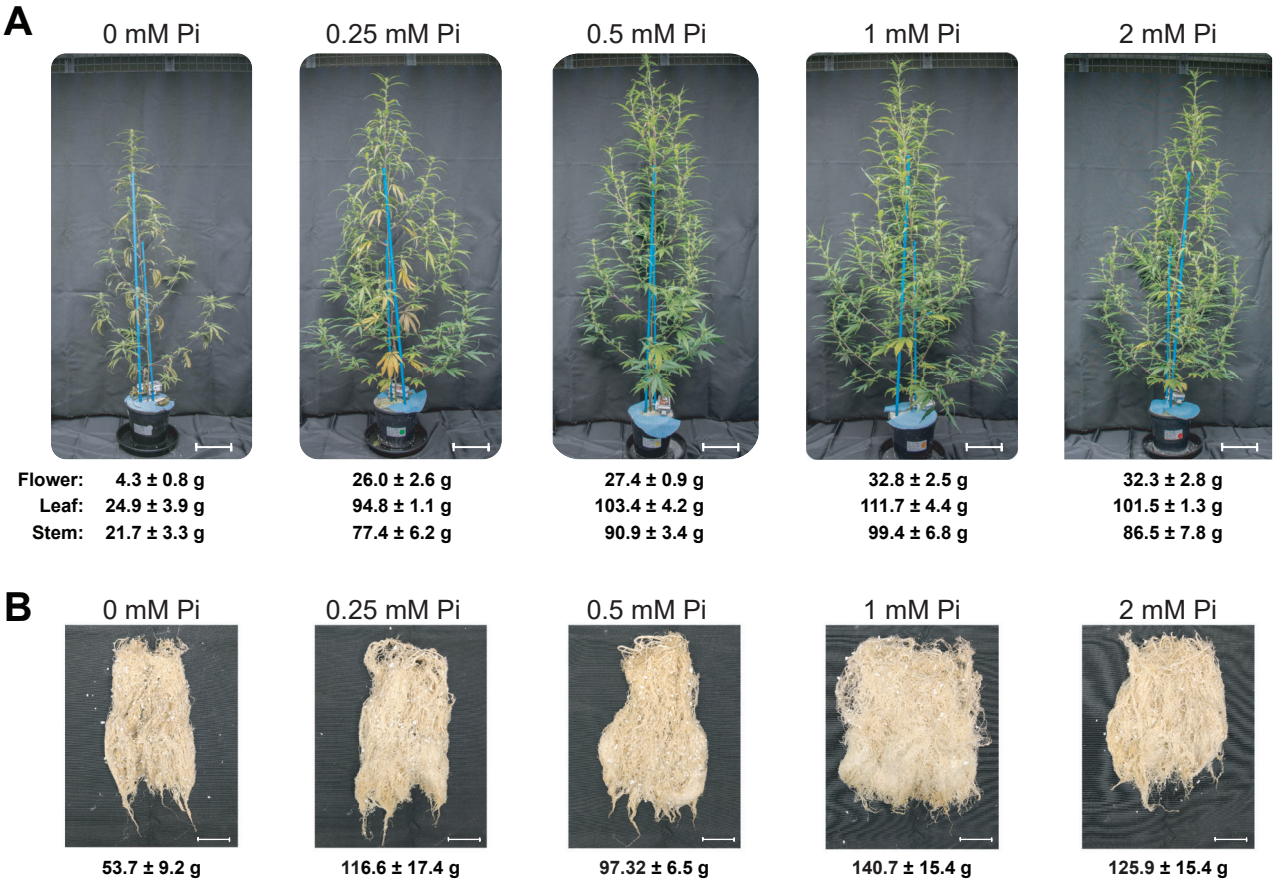

Figure 1. Phenotypic response of female hemp plants to changes in Pi supply. Shown are images of representative clonal plants for each treatment prior to final destructive harvest at 42 DAT. (**A**) Plant morphology across treatments. Chlorosis gradient increased in senescing leaves along the main stem with decreasing Pi supply. Scale bar represents 20 cm. (**B**) Root ball morphology across treatments. Scale bar represents 5 cm. Organ biomass in g FW plant^{-1} is given below each panel, as mean ± SE (n = 3 plants per treatment).

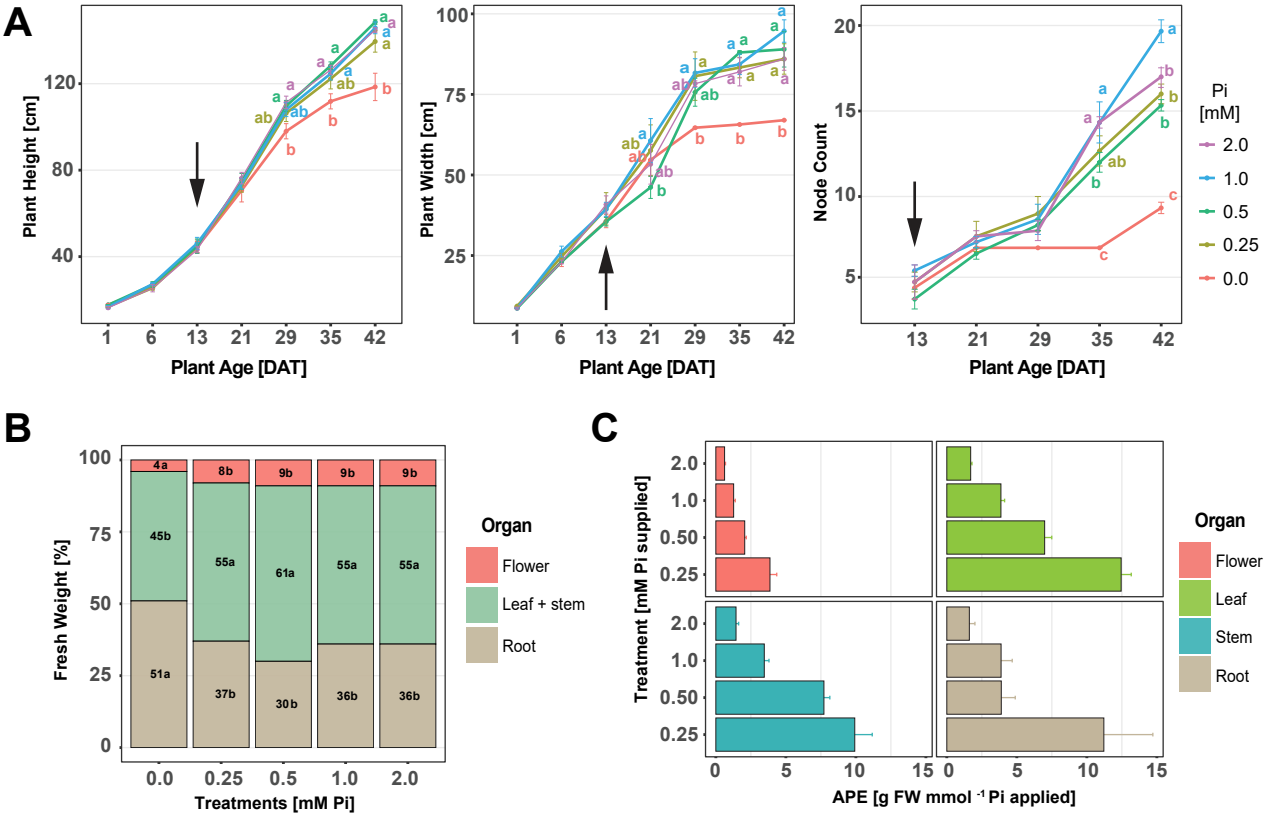

Figure 2. Morphological response to Pi supply across timepoints. (A) Changes in plant height, plant width and node count were determined at indicated time points across treatments. DAT refers to days after transfer of rooted female cuttings into pots. Arrows indicate timepoint when Pi treatments were initiated. **(B)** Biomass partitioning across organ types, as a percentage of total fresh biomass for each treatment. Vegetative organs are stem and leaves combined. **(C)** Agronomic phosphate efficiency (APE) across treatments in comparison to 0 mM Pi supply. APE across is highest at 0.25 mM Pi supply and decreases with higher Pi supply across organs. Given are means ± SE, n = 3 plants per treatment. Letters denote significant difference (ANOVA, Tukey's HSD, $p < 0.05$) between treatments and / or organ types. Also refer to Supplemental Tables 1 and 2 for supporting datasets.

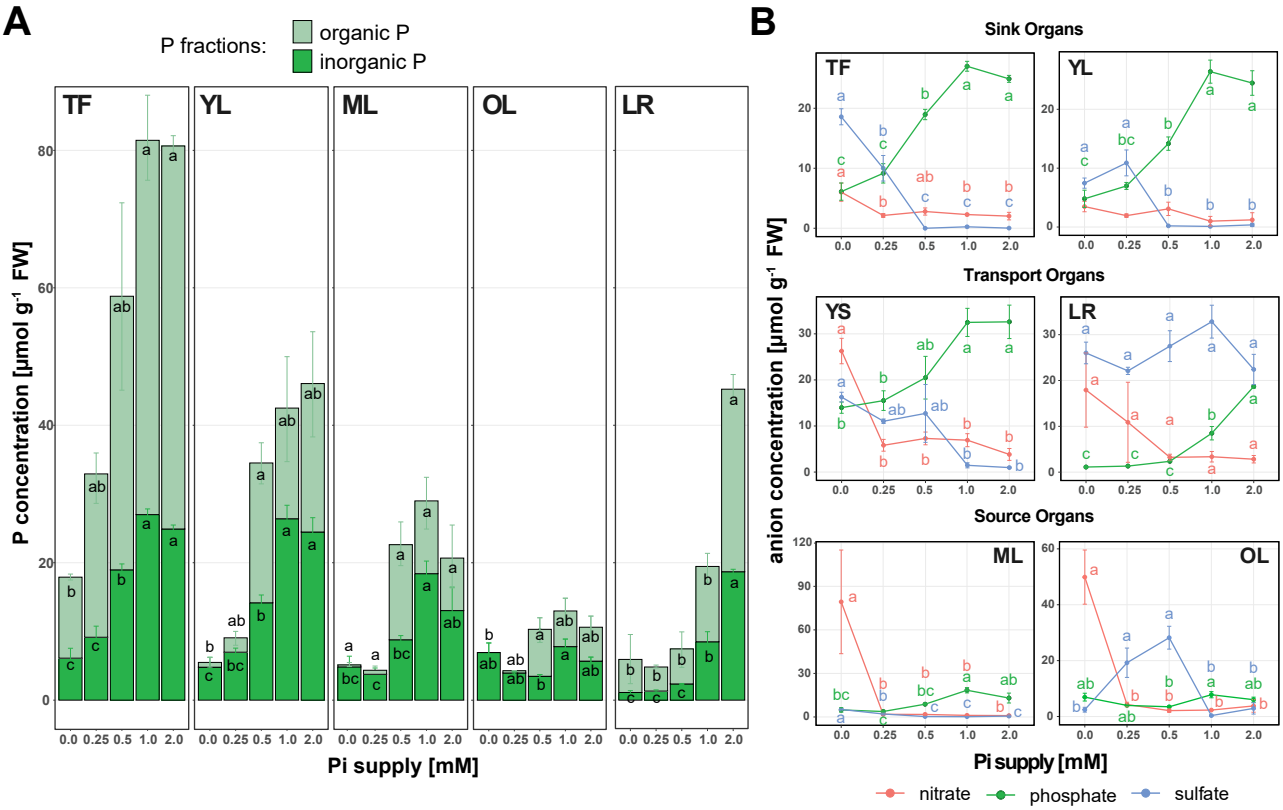

Figure 3. Pi supply affects Pi assimilation as well as inorganic storage pools across organ types.
(A) Concentrations of inorganic and organic P across organ types and Pi treatments. **(B)** Concentrations of nitrate, phosphate and sulfate across organ types and Pi treatments. Letters denote statistical significance across treatments (ANOVA/TUKEY HSD, $p < 0.05$). Given are means ± SE (n = 3 plants per treatment). See Supplementary Table S3 for data and statistical analyses. TF, terminal flower; YL, young leaf; ML, mature leaf; OL, old leaf; LR, lateral root; YS, young stem.

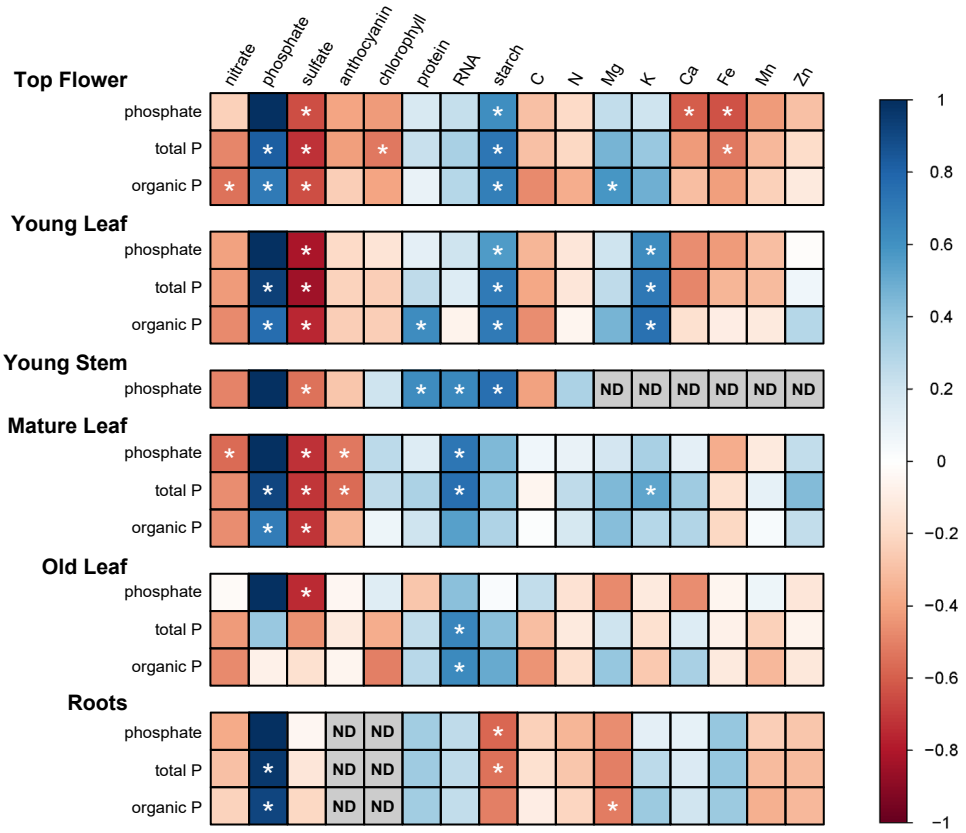

Figure 4. Correlation matrix of measured metabolites and P fractions across organ types. Pearson's correlation to assess relationship between concentrations of indicated metabolites and different P fractions for given organs. Asterisks denote significant correlations ($p < 0.05$) and colour scale indicates correlation coefficient. ND: not determined.

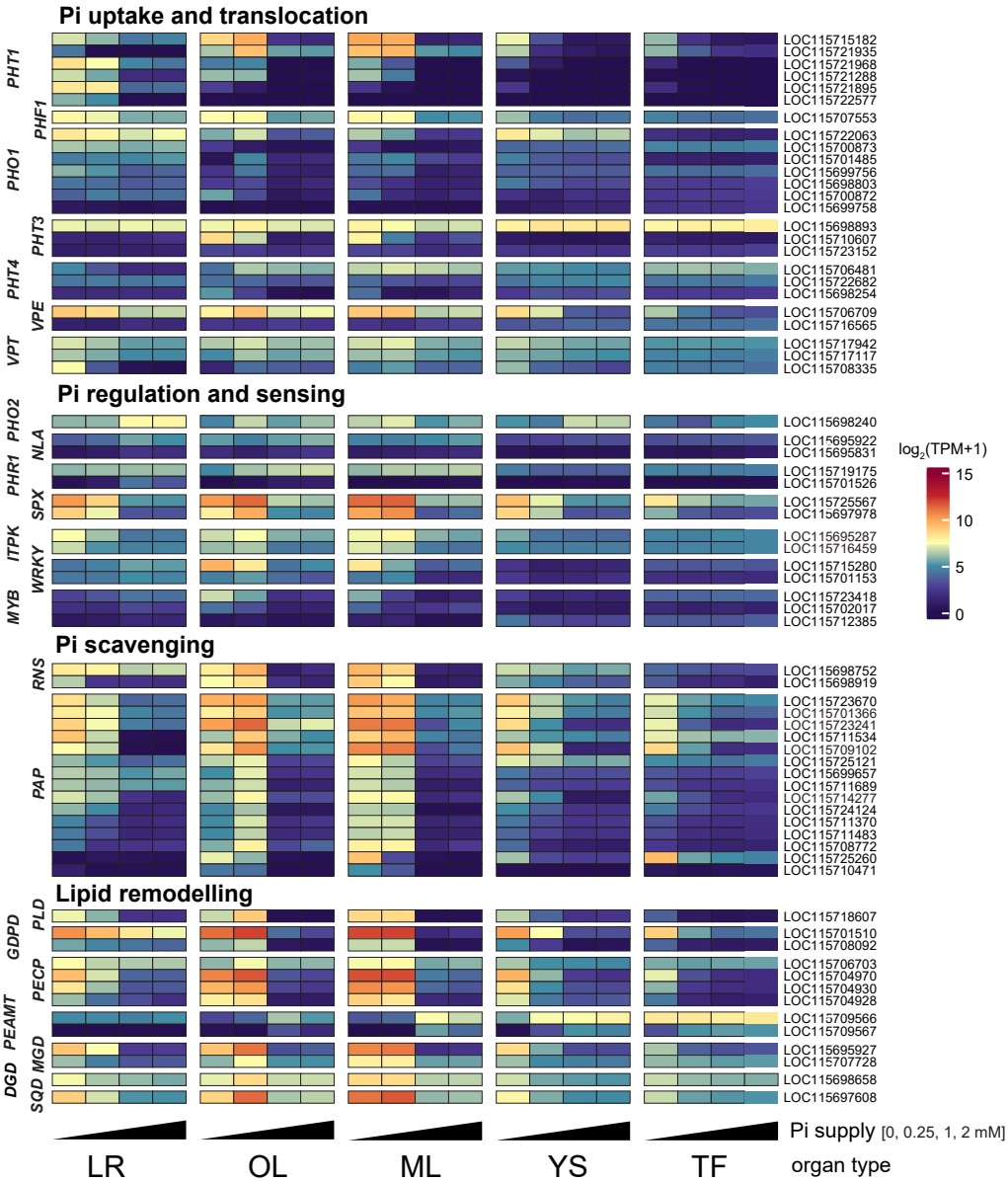

Figure 5. Transcriptional response of curated PSR genes. *Cannabis* homologs of known PSR genes in Arabidopsis were categorised into functional groups. PSR transcript abundance across organ types (LR, lateral root; OL, old leaf, ML, mature leaf; YS, young stem; TF, terminal flower) is expressed as log2 transformed TPM values. Transcriptomic data and curated gene list are provided in Supplemental Tables 5 to 7. The cs10 reference gene IDs are shown on the right. Abbreviations for gene family names shown to the left of the panel: *PHT, PHOSPHATE TRANSPORTER; PHF1, PHOSHATE TRANSPORT FACILITATOR1; PHO1, PHOSPHATE1; VPE, VACUOLAR PHOSPHATE EFFLUX TRANSPORTER; VPT, VACUOLAR PHOSPHATE TRANSPORTER; PHO2, PHOSPHATE2; NLA, NITROGEN LIMITATION ADAPTATION; PHR1, PHOSPHATE STARVATION RESPONSE1; SPX, SPX DOMAIN GENE; ITPK, INOSITOL 1,3,4-TRISPHOSPHATE 5/6-KINASE; WRKY, WRKY DNA-BINDING PROTEIN; MYB, MYB-DOMAIN PROTEIN; RNS, RIBONUCLEASE; PAP, PURPLE ACID PHOSPHATASE; PLD, PHOSPHOLIPASE D; GDPD, GLYCEROPHOSPHODIESTER PHOSPHODIESTERASE; PECP1, PHOSPHOETHANOLAMINE/PHOSPHOCHOLINE PHOSPHATASE1; PEAMT, PHOSPHOETHANOLAMINE N-METHYLTRANSFERASE; MGD, MONO-GALACTOSYL DIACYLGLYCEROL SYNTHASE; SQD, SULFOQUINOVOSYL-DIACYLGLYCEROL SYNTHASE.*

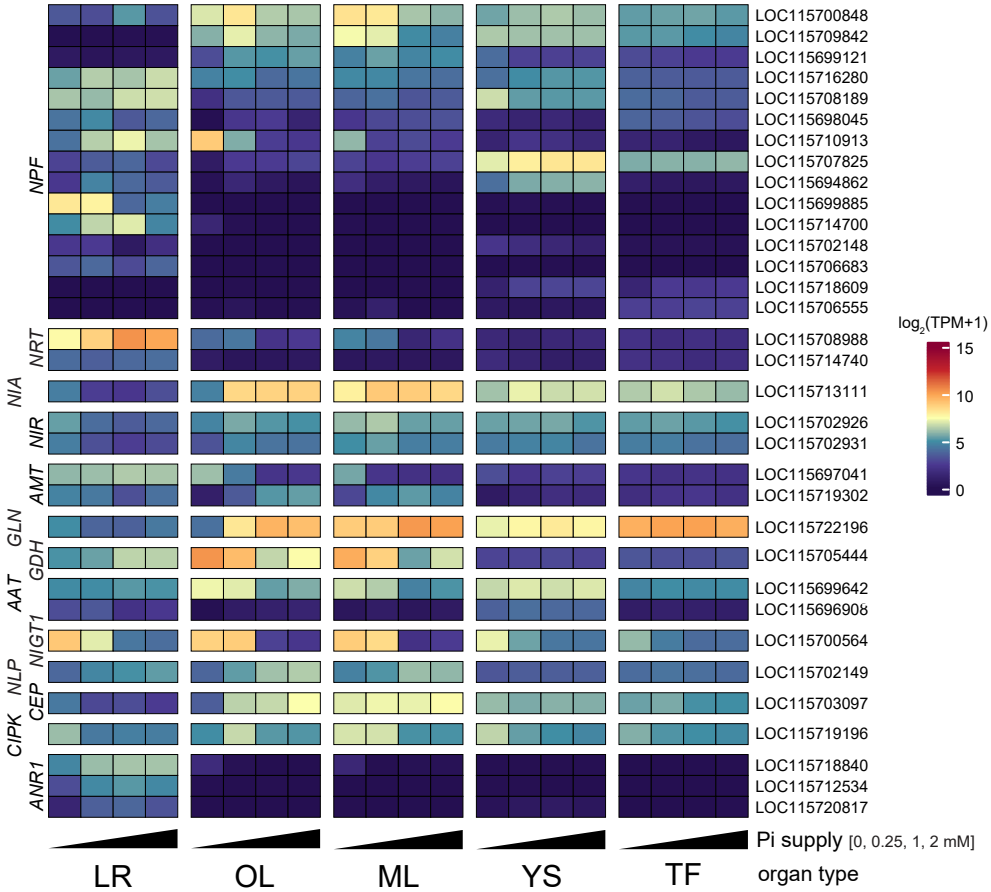

Figure 6. Transcriptional response of curated genes involved in N assimilation and metabolism in hemp. Shown are transcript abundances for *Cannabis* homologs of genes with a known role in N assimilation, metabolism and their transcriptional regulation in Arabidopsis. The heatmap represents log-transformed TPM ($\log_2$(TPM+1)) across organ types (LR, lateral root; OL, old leaf, ML, mature leaf; YS, young stem; TF, terminal flower). Transcriptomic dataset and fully curated gene list is provided in Supplemental Tables 5-7. cs10 genome gene IDs are shown on the right. Abbreviations for gene family names shown on the left of the panel: *AMT, AMMONIUM TRANSPORTER; NRT, NITRATE TRANSPORTER; ANR1, ARABIDOPSIS NITRATE REGULATED1; NITRITE REDUCTASE, NIR; NITRATE REDUCTASE, NIA; GLUTAMINE SYNTHETASE, GLN; NITRATE-INDUCIBLE GARP-TYPE TRANSCRIPTIONAL REPRESSOR1, NIGT1; NIN-LIKE PROTEIN, NLP; NRT1/PEPTIDE TRANSPORTER, NPF; GLUTAMATE DEHYDROGENASE, GDH; ASPARTATE AMINOTRANSFERASE, AAT; C-TERMINALLY ENCODED PEPTIDE, CEP; CALCINEURIN B-LIKE PROTEIN-INTERACTING PROTEIN KINASE, CIPK*.